2016

Regenerative damping - Analysis of expected benefits on CO2 emissions and ride-comfort improvement

Marco Di Vittorio
University of Windsor

Regenerative damping - Analysis of expected benefits on CO_2 emissions and ride-comfort improvement

by

Marco Di Vittorio

A Thesis
Submitted to the Faculty of Graduate Studies
through the Department of Mechanical, Automotive, and Materials Engineering
in Partial Fulfillment of the Requirements for
the Degree of Master of Applied Science
at the University of Windsor

Windsor, Ontario, Canada
2016

Regenerative damping - Analysis of expected benefits on CO_2 emissions and ride-comfort improvement

by

Marco Di Vittorio

APPROVED BY:

Dr. N. Kar
Department of Electrical and Computer Engineering

Dr. J. Johrendt
Department of Mechanical, Automotive, and Materials Engineering

---

Dr. B. Minaker, Advisor
Department of Mechanical, Automotive, and Materials Engineering

August 29, 2016

Declaration of Originality

I hereby certify that I am the sole author of this thesis and that no part of this thesis has been published or submitted for publication.

I certify that, to the best of my knowledge, my thesis does not infringe upon anyone's copyright nor violate any proprietary rights and that any ideas, techniques, quotations, or any other material from the work of other people included in my thesis, published or otherwise, are fully acknowledged in accordance with the standard referencing practices. Furthermore, to the extent that I have included copyrighted material that surpasses the bounds of fair dealing within the meaning of the Canada Copyright Act, I certify that I have obtained a written permission from the copyright owner(s) to include such material(s) in my thesis and have included copies of such copyright clearances to my appendix.

I declare that this is a true copy of my thesis, including any final revisions, as approved by my thesis committee and the Graduate Studies office, and that this thesis has not been submitted for a higher degree to any other University or Institution.

Abstract

In the last years, energy efficiency has been of great concern due to the increasing number of vehicles that is on the road. For this reason, energy recovery systems are being developed. Regenerative dampers, which are a category of these devices, are able to harvest energy coming from the road irregularities. In this way, the energy is no more dissipated into heat by the damper, but it is recovered through an hydraulic pump rigidly connected to an electric generator.

The goal of this study is to develop a Matlab® and Carsim® full-vehicle model of a segment C car with regenerative hydraulic dampers in order to evaluate the improvements that could be obtained in terms of harvested energy and, also, in terms of vehicle comfort and dynamics by properly tuning the damper device. Moreover, an analysis on the CO_2 savings will be carried out, considering several driving conditions, with different road roughness profiles and vehicle velocities.

To my parents.The reason of what I become today.

Acknowledgements

This thesis is the outcome of a Double Master Degree Program between Politecnico di Torino and University of Windsor and one of the leading group in automotive industry, Fiat Chrysler Automobiles. This was made possible thanks to the effort of people that believe in this program. For this reason, I'd like to express my appreciation to those people, who played a very important role in the coordination of the program, Prof. Giovanni Belingardi from Politecnico di Torino, Dr. Andrzej Sobiesiak from University of Windsor, Mohammed Malik from FCA Canada and Edoardo Rabino from FCA Italy.

I would like to express my gratitude to my academic advisors, Prof. Nicola Amati from Politecnico di Torino and Dr. Bruce Minaker from University of Windsor, who supervised my activities and offered their very important support throughout all my work. I also want to express my appreciation to my industrial advisor Michele Ieluzzi from Centro Ricerche Fiat for his availability and precious suggestions, and Brian Pecheniuk from Chrysler Technical Center.

Now I would like to thank some people that were very important during these last five years of university. First of all some of my roommates in Torino during my bachelor and 1st year of master degree, Vins, Angelo, Carlo, Stefano, and Gli Amici Delle Molinette (Cosimo, Gaspare and Lorenzo). A special thanks to Lorenzo that had to stand my presence for three years and to Stefano G. for all the beautiful projects we made and for all the experiences we lived together.

Last but not least, I say a big thank to my house mates in Windsor, Marco, my fall semester kitchen mate, Davide Luigi 'the best', my sponsor, Davide Ruben, my teammate, J, my winter semester kitchen mate, Mirko, the story teller. Thanks to all of you guys, it's also thank to you that this experience has been unforgettable.

Thank you also to our Rochester friends Marcello, for being my photography mentor, and Nick for being always available in receiving my packages.

My whole love and gratitude goes to my parents Ennio and Patrizia, my little sister Natalia and all my uncles, aunts and the people who believed in me during all these years. I owe to them who I am and who I will be in the future. I will for ever be grateful to you.

"*Learn from yesterday, live for today, hope for tomorrow. The important thing is not to stop questioning.*"

Albert Einstein

Table of Contents

List of Tables

List of Figures

List of Appendices

List of Abbreviations

AC	Alternate Current
CG	Center of Gravity
DC	Direct Current
DCM	Discontinuous Conduction Mode
DOT	Department of Transportation
EC	European Commission
EHA	Electro Hydraulic Actuator
EMF	Electromotive Force
ICE	Internal Combustion Engine
ISO	International Organization for Standardization
MR	Magneto rheological
PID	Proportional Integral Derivative
$PMSM$	Permanent Magnet Synchronous Machine
PSD	Power Spectral Density
RHI	Road Handling Index
RMS	Root Mean Square
SMR	Switch Mode Rectifier

List of Symbols

η_{alt}	Alternator efficiency
η_{conv}	Efficiency of power converter
η_b	Ball screw efficiency
η_g	Transmission efficiency
η_m	Mechanical efficiency
η_v	Volumetric efficiency
ν	Spatial frequency
σ	Electrical conductivity
ϕ	Magnetic flux
ω	Pump rotation speed
ω_0	Cutoff frequency
ω_m	Angular velocity of the pump
ω_n	Nominal rotation speed
a	Distance from center of gravity to front axle
a_b	Width of piezoelectric bar
A_{nr}	Area of the damper piston without considering the rod
A_r	Area of the damper piston considering the rod
b	Distance from center of gravity to rear axle
B	Magnetic flux
B_r	Magnetic flux in radial direction
c	Damping coefficient
c_2	Damping coefficient between m_1 and m_2

c_{max}	Maximum damper coefficient
c_v	Electrical capacity of piezoelectric bar
C_eq	Equivalent damping ratio
C_s	Velocity feedback gain of sprung mass
C_u	Velocity feedback gain of unsprung mass
CF	Conversion factor from fuel consumption to CO_2
CO_2	Carbon dioxide
D	Duty cycle
d_{33}	Piezoelectric constant in the polling direction
e	Error signal
E	Electromotive force
E_p	Young's modulus
f	First natural vibration frequency
f_{sw}	Switching fequency
F_d	Damper force
F_s	Spring force
F_z	Ground normal force
F_{z1}	Ground normal force of front axle
F_{z2}	Grounf normal force of rear axle
g	Gravity acceleration
G_r	Road roughness coefficient
h	Height of piezoelectric bar
i_d	Direct-axis current
i_q	Quadrature current
I	Current
I_d	Equivalent inertia
I_n	Nominal current
J	Moment of inertia
J_b	Ballscrew inertia
J_g	Gearbox inertia

J_m	Motor inertia
k	Spring stiffness coefficient
k'	Equivalent stiffness coefficient of piezoelectric bar
k_1	Tire stiffness
k_2	Spring stiffness coefficient
k_e	Motor voltage constant
k_g	Transmission ratio form pinion gear to generator rotor
k_h	Pressure drop coefficient
k_m	Motor constant
k_t	Motor torque constant
k_{tot}	Total stiffness coefficient of piezoelectric bar
l	Length of inductor
L	Inductance
l	Wheelbase
L_1	Length of long moment arm
L_2	Length of short moment arm
l_b	Lead of the ball screw
m	Vehicle mass
m_1	Unsprung mass of quarter car model
m_2	Sprung mass of quarter car model
m_s	Sprung mass
m_u	Unsprung mass
$\dot{z}_M$	Velocity of suspended mass
$\dot{z}_m$	Velocity of unsprung mass
n	Ratio between L_1 and L_2
p	Number of paired poles
P	Peak power
P_1	Pressure in chamber A
P_2	Pressure in chamber B
P_{eha}	Pressure of the EHA

P_h	Harvested power
P_{or}	Pressure through the orifices
q	Pump capacity
Q_g	Volumetric flow through the pump
Q_{pump}	Oil flow rate through the pump
Q_{top}	Volumetric flow passing through the valve between chamber A and B
R	Loop resistance
R_e	External resistance
r_i	Internal resistance
S	Spatial frequency
S_{CO_2}	CO_2 saving
t_0	Simulation start time
t_{end}	Simulation ending time
T_m	PMSM output torque
T_{pump}	Pump output torque
u	Control input
U_{emf}	Back electromotive force voltage
U_{output}	Output voltage
U_n	Input voltage
v	Relative axial velocity
v_{in}	Input damper velocity
V	Vehicle speed
$V_{battery}$	Battery voltage
V_d	Direct-axis voltage
V_{in}	Input voltage
V_m	Validation metric
V_{PE}	Marginal engine's efficiency
V_q	Quadrature voltage
Z_L	Vertical displacement of the vehicle
Z_r	Road surface change

Z_s	Suspension supplement displacement
z_u	Vertical displacement of unsprung mass
z_w	Vertical displacement of the wheel

Chapter 1

Introduction

Vehicle energy harvesting and the improvement of energy efficiency have been of concern for the last two decades. In recent years, the increasing number of vehicles on the road has lead to a dramatic increase in fossil fuel demand [1]. A high rate of consumption results in excessive carbon footprint and emissions. Since 2013, transportation accounts for about 23% of the global CO_2 emissions. In particular, road transportation is responsible for more than two third of the entire amount of CO_2 due to transportation [2]. Some of the

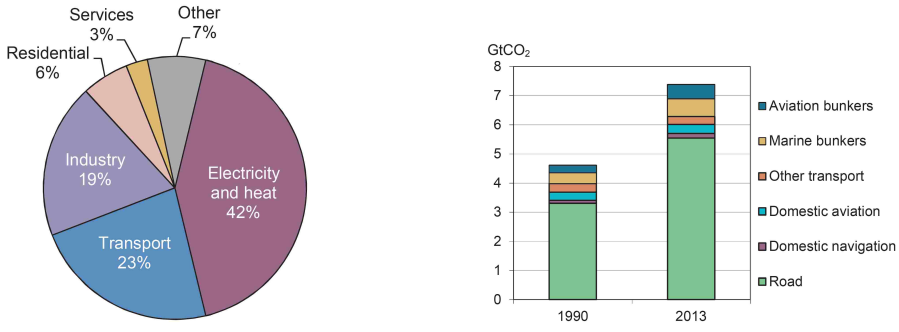

(a) *World CO_2 emissions by sector in 2013*

(b) *CO_2 emissions from transport*

Figure 1.1: *CO_2 emission trends (figure reproduced from [1])*

advanced technologies to improve vehicle fuel efficiency, in order to reduce emissions, are

regenerative systems. The most popular regenerative systems are regenerative braking and regenerative suspensions. The former system has been widely studied and is currently used by different car manufacturers. The latter, instead, which is the subject of this work, is not yet commercialized and it still needs some further investigations. The main goal of a vehicle suspension system is the reduction of vibrations from road roughness, in order to have good ride comfort and to maintain a good tire-ground contact to have good handling capabilities. A conventional shock absorber dissipates the mechanical energy into heat with a fixed damping behavior. Conversely, a regenerative damper converts the mechanical energy into electrical energy that can be then used to charge the battery (Figure 1.2). However, this type

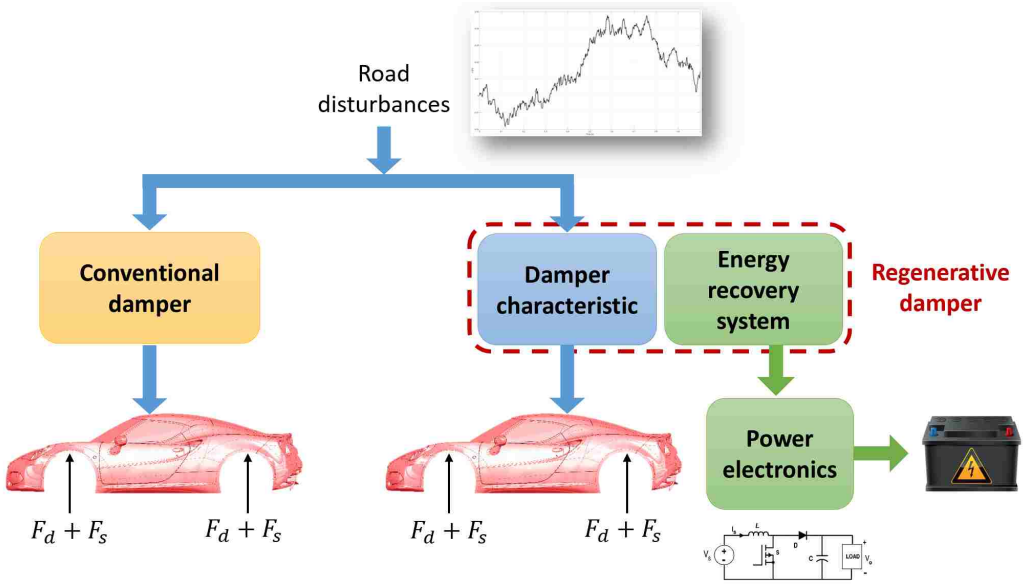

Figure 1.2: *Comparison between conventional and regenerative shock absorbers*

of shock absorber has some challenges that must be faced before considering its introduction in mass production vehicles.

1.1 Objectives of the work

The first step of the project is to provide a summery of the state of art of the technologies that have been studied in past research, providing a classification of the most relevant solutions, highlighting pros and cons of each solution. The main part of the project is

then aimed at evaluating the final benefits that a regenerative damper could provide. As a first analysis, the amount of energy that can ideally be recovered from the damper is analyzed, considering different driving conditions. Then, a model of the regenerative damper is included inside the car model and the efficiency of the damper is evaluated. Moreover, an appropriate strategy will be studied in order to reach the best possible trade-off between energy harvesting and ride comfort.

1.2 Methodology

In order to simulate the aforementioned model, both CarSim®and Matlab®software are used. In particular:

- CarSim®software will be used to simulate the full vehicle model. The vehicle analyzed is an Alfa Romeo Giulietta (segment C).
- Matlab®software is used to simulate the dampers' behavior. All the damper models are inside the Simulink environment.

During the simulations, the two simulations run in parallel, and continuously exchange information coming from the damper modeled in Simulink. After the simulation, both the outputs from Simulink regarding regeneration and the outputs from CarSim regarding the vehicle behaviour are available.

1.3 Thesis organization

The thesis is organized as listed below:

Chapter 2 the literature review and the state of art of regenerative suspensions are presented. Small remarks on vehicle dynamics are also present, in particular vertical dynamics and road profile analysis. Some statistical data concerning vehicle usage are also provided.

Chapter 3 the creation of the model and the description of both the full vehicle and damper model is shown. Moreover, a characterization of the road profiles used during

the simulation is provided. The integration of the damper model inside the full vehicle will occur, as well as the description of the control strategy.

Chapter 4 the results coming from the simulations with both conventional and regenerative dampers are presented. The amount of energy that is recovered is evaluated according to vehicle usage statistics. The analysis of the results obtained is carried out and the benefits attained thanks to the use of this new type of damper are investigated.

Chapter 5 the conclusions and findings of the research are summarized and future recommendations are presented.

Chapter 2

Literature review

2.1 Vehicle suspension system

The vehicle suspension system is responsible for driving comfort and safety as the suspension carries the vehicle body and transmits all forces between the body and the road. It consists of wishbones, a spring, and the shock absorber to transmit and also filter all forces between the body and road. The spring carries the body mass and isolates the body from road disturbances and thus contributes to drive comfort. The damper contributes to both driving safety and comfort. Its task is the damping of body and wheel oscillations, where the avoidance of wheel oscillations directly refers to drive safety, as a non-bouncing wheel is the condition for best transferring road-contact forces. These two characteristics will now be analyzed more deeply.

Driving Safety It is the result of a harmonious suspension design in terms of wheel suspension, steering and braking, and is reflected in an optimal dynamic behavior of the vehicle. Tire load variation is an indicator for tire-road contact and can be used to determine a quantitative value for safety.

Driving Comfort It results from keeping the physiological stress that the vehicle occupants are subjected to by vibrations, noise, and climatic conditions down to as low a

level as possible. The acceleration of the body is an obvious quantity for the motion and vibration of the car body and can be used to determine a quantitative value for driving comfort.

In order to improve the ride quality, it is necessary to isolate the body, also called the sprung mass, from the road disturbances and to decrease the resonance peak of the sprung mass near $1\,Hz$, which is known to be a sensitive frequency to human body. In order to improve the ride stability, it is important to keep the tire in contact with the road surface, and therefore to decrease the resonance peak near $10\,Hz$, which is the resonance frequency of the unsprung mass. However, ride quality and drive stability are two conflicting fields, so a compromise has to be found. For this reason, several types of suspensions have been designed, in order to obtain the best from both the required fields. These suspensions will be analyzed in the following section.

2.1.1 Types of vehicle suspension system

Nowadays, many studies are focused on research into vehicle suspension systems, both to improve handling performance and to try to recover a part of the energy that is dissipated in the suspension itself. The former kind of suspension is called *active*, the latter *regenerative*. In the following, the two categories will be analyzed in detail. A suspension system is essential to isolate the frame of the vehicle from the disturbances coming from the road. The damper has the role to reduce the disturbances coming from the road by smoothing out the shock, so it dissipates energy. However, a suspension system has also a fundamental role concerning the vehicle dynamic behavior. Advantages on handling performance can be obtained by controlling the amount of damping. According to the amount of controllability that can be obtained on the system, the suspension systems are categorized as *passive*, *semi-active* and *active*.

2.1.2 Passive suspension systems

Passive suspension systems are characterized by complete lack of additional energy required for their operation. The spring and damping properties of these systems are static and are described by constant force-displacement and force-velocity curves. These characteristics

are determined by the designer of the suspension, according to the design goals and intended application. A heavily damped suspension will yield good vehicle handling, but also transfers much of the road input to the vehicle body. When the vehicle is traveling at low speed on a rough road or at high speed in a straight line, this will be perceived as a harsh ride. A lightly damped suspension will yield a more comfortable ride, but can significantly reduce the stability of the vehicle in turns or lane change maneuvers. According to the segment of the vehicle to which they are applied, a compromise between ride comfort and ride handling needs to be found, since the suspension characteristics remain constant for all road profiles.

2.1.3 Semi-active suspension systems

In semi-active suspensions, an actuating force is generated by a controller. In this case, the damping characteristic can be changed to some extent. These suspensions have better performance than passive suspension systems. The adjustable damping characteristic can be obtained through the use of different technologies, such as Electro-Rheological and Magneto-Rheological fluids, solenoid-valves and piezoelectric actuators.

2.1.4 Active suspension systems

An active suspension system is able to generate forces between the vehicle's body and wheels that are fully independent of the current suspension travel direction. The application of forces requires a non-negligible amount of energy, thus it requires an external power source.

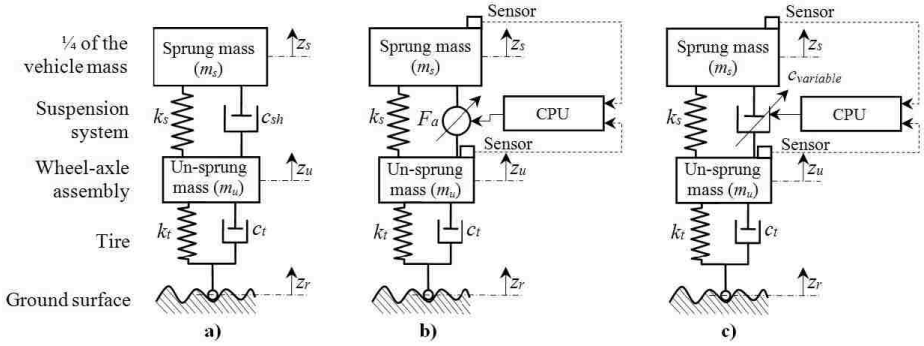

Figure 2.1: *Quarter vehicle models: a) Passive, b) Active, c) Semi-Active suspension systems*

2.2 Passive damper devices

Vehicle shock absorbers are actually vibration dampers. Vibration dampers are arranged parallel to the vehicle suspension and have the following tasks [6]:

- to dampen oscillations and vibrations of the vehicle's body caused by uneven roads or driving conditions
- to quickly reduce and eliminate road-induced wheel and axle vibration in order to provide constant contact between the tire and the roadway. This helps ensure good tracking and braking performance

When the vehicle drives over a bump, the suspension springs and vibration dampers are compressed. The resulting shock to the vehicle is absorbed by the suspension. The suspension prevents the sprung mass from making contact with the unsprung mass. The springs, however, tend to relax again, thereby releasing the energy stored within them. In order to quickly reduce and eliminate this springing oscillation between the axle and body, the chassis is equipped with dampers. Sprung and unsprung masses vibrate in different frequency ranges.

2.2.1 Monotube shock absorbers

In a monotube shock absorber, the main chamber and the oil supply chamber are located in the same single cylinder tube. The oil and gas are separated by a moving separating piston with an O-ring seal. The system is shown in Figure 2.2. The damping valves for both rebound and compression stages are located on the piston. When the vehicle suspension rebounds, the piston valve, which is located at the bottom of the piston, applies resistance to the oil as it flows downward. The gas pressure is reduced by an amount which corresponds to the lost piston rod volume. When the vehicle suspension compresses, the oil is forced from the bottom chamber through the piston and the valve located on top of the piston.

2.2.2 Twin-tube shock absorbers

In a twin-tube shock absorber, the main cylinder and the outer tube form two chambers: the main chamber in the main cylinder and the oil supply chamber located between the

Figure 2.2: *Monotube damper (figure reproduced from [3])*

main cylinder and the outer tube. The movement of the piston and piston rod takes place in the main chamber. The annular oil supply chamber compensates for any oil volume changes in the main chamber caused by the piston rod movement. The extension and retraction of the piston rod causes the gas pressure in the oil supply chamber to increase or decrease. This change in pressure corresponds to the volume of the oil exchanged. For damping, two valves are used: the piston valve and the bottom valve. The system is shown in Figure 2.3. These valves consist of an arrangement of spring disks, helical springs, and valve bodies with

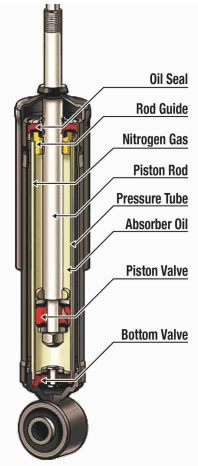

Figure 2.3: *Twin-tube shock absorber (figure reproduced from [4])*

restriction holes. When the vehicle suspension rebounds, the piston valve alone provides

damping by applying resistance to the oil flowing downwards from the chamber above the piston. This resistance slows the upward movement of the piston. The oil required in the main chamber flows freely from the supply chamber through the open check valve located in the bottom valve. When the vehicle suspension is compressed, damping is provided by a combination of the bottom valve and, to a certain extent, the flow rate resistance of the piston in the compression direction. During compression, the oil displaced by the piston rod flows into the supply chamber. The bottom valve applies resistance to this flow, slowing its movement. The piston valve provides a small resistance which can be adjusted according to the damping requirement.

2.2.3 Comparison of passive damper types

The specific properties of mono-tube and twin-tube shock absorbers can be summarized as follows:

- Due to the separation of gas and oil, the valve function of a monotube damper tends to cavitate slightly less than that of a twin-tube damper. As a result, a monotube damper functions slightly better for short strokes
- Twin-tube dampers use two separate valves for compression and rebound. This allows more flexibility when specifying the characteristic curves. The compression damping of a monotube shock absorber is limited by the gas pressure which helps absorb the damping forces
- The pressurized (preloaded) seals in a monotube damper result in slightly higher friction
- The position of the compensation chamber at the end of a monotube damper results in a thinner but longer package
- There are no restrictions on the installation position of a monotube damper, but a twin-tube damper must remain approximately vertical
- Monotube dampers contain fewer parts than twintube dampers, and weigh slightly less as a result

2.3 Regenerative suspension systems

It is well known that when vehicles travel on the road, they are subjected to forces coming from the road irregularities, braking and acceleration forces, cornering forces and other disturbances that can affect comfort and drive ability. As discussed before, the use of active suspension systems improves ride quality and handling, but with the disadvantage of a great amount of energy needed. For this reason, regenerative suspensions have been proposed, in order to harvest energy while reducing vibrations [4,5]. The research done on energy harvesting dampers shows that approximately $200\,W$ of power are dissipated by dampers of passenger cars at $30\,mph$ on highway pavement roughness [6]. Several energy harvesting dampers have been studied; these can be divided into different categories: piezoelectric, electromagnetic and hydraulic devices.

2.3.1 Piezoelectric damper devices

Piezoelectric materials are able to convert strain energy into electricity. These materials create a voltage under an applied strain and vice versa [7]. These piezoelectric devices have many drawbacks, due to the fact that generally strains are very small, thus reducing the amount of energy that could be recovered, and also the voltage produced by piezoelectric materials has a decay time. In [22] a dual-mass piezoelectric bar harvester is developed for energy harvesting from ambient vibrations of a vehicle suspension system. The piezoelectric bar transducer model consists of a spring, a lever consisting of both a long and a short moment arm and the piezoelectric bar itself. The results obtained show that the RMS (root mean square) of the generated power increases with an increase in the velocity of the vehicles and the class of road surface according to the ISO standard, an increase in the ratio of the moment arms of the lever, and a decrease in the width of the piezoelectric bar. The piezoelectric bar transducer model is schematically illustrated in Figure 2.4. It consists of a spring with a stiffness coefficient k, a lever AB consisting of a long moment arm of AC with a length L_1 and a short moment arm BC with length L_2, a fixed hinge for restricting linear displacement of the lever at point C, and a piezoelectric bar with a Young's modulus E_p, a width a_b and height h. The equivalent stiffness coefficient of the device assembled by

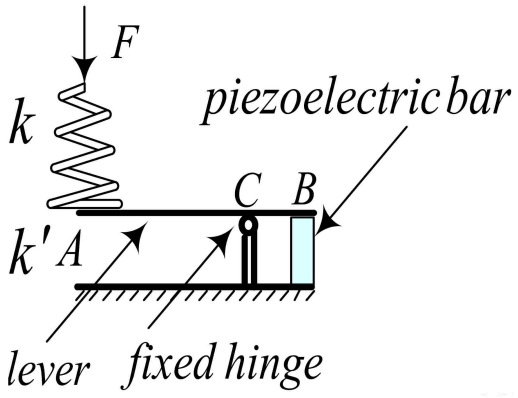

Figure 2.4: *Piezoelectric regenerative damper (figure reproduced from [22])*

the lever and the piezoelectric bar is

$$k' = \frac{E_p a_b^2}{n^2 h} \tag{2.3.1}$$

where n is the ratio between the two lengths L_1 and L_2. Therefore, the total stiffness coefficient of the piezoelectric bar is equal to

$$k_{tot} = \frac{kk'}{k + k'} \tag{2.3.2}$$

Its characteristics have been simulated in a quarter car model by X.D.Xie and Q. Wang [22]. The model considered is characterized by the unsprung mass m_1, the stiffness of the tire k_1, the sprung mass m_2, a spring k_2 and a damper c_2 connecting the two masses m_1 and m_2. While the value of k_2 is given by the total stiffness of the piezoelectric bar from Equation 2.3.2, the damping coefficient c_2 can be derived as follows

$$c_2 = \frac{n^2 d_{33}^2 k_2^2}{\pi^2 c_v f} \tag{2.3.3}$$

where d_{33} is the piezoelectric constant in the polling direction, c_v is the electrical capacity of the piezoelectric bar and f is the first natural vibration frequency of the vehicle suspension. The computation results show that the RMS of the power increases with an increase in the ratio of the moment arms of the lever, and a decrease in the width of the piezoelectric bar.

2.3.2 Electromagnetic damper devices

Electromagnetic devices involve the conversion of kinetic energy into electrical energy. A voltage is produced between two ends of the device by the movement of a magnetic field.

The movement of the damper generates, from Faraday's law of induction, an induced electromotive force proportional to the derivative of the magnetic flux (ϕ) through the circuit with respect to time.

$$E = -\frac{d\phi}{dt} \tag{2.3.4}$$

This kind of device can be used both as actuation and regenerative device. The drawback of this device is given by their dimensions, which are much larger than a regular damper. This could be a limiting factor in case of a small space available in the suspension system. The electromagnetic suspension system consists of a linear electromagnetic motor. The electromagnetic motor has the role of converting the energy of the suspension into electrical power. This actuator is made of adjacent magnets facing each other and equally spaced [4]. The maximum current generated by this device is given by:

$$I = \frac{V}{R} = \sigma B_r v A \tag{2.3.5}$$

where σ is the electrical conductivity, B_r the magnetic flux in the radial direction and v is the relative axial velocity and A is the cross-sectional area. Lei Zuo *et al.* [9] created a prototype, evaluating the voltage and power generated. The shock absorber is in the configuration of a linear generator, as shown in Figure 2.5. The magnets are arranged with

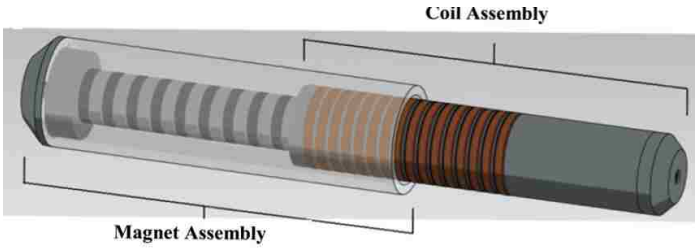

Figure 2.5: *Diagram of the linear electromagnetic shock absorber (figure reproduced from [9])*

like-poles of adjacent magnets facing each other to redirect the magnetic flux in the radial direction. A concentric outer cylinder made of high magnetically permeable material is used to reduce the reluctance of the magnetic loops, to further increase the flux density in the coils. The EMF voltage V generated by a conductor of length l moving in a magnetic field B, at a constant velocity v is given by

$$V = Bvl \tag{2.3.6}$$

and the maximum current is given by Equation 2.3.5. So, the peak power P can be calculated as

$$P = VI = B_r^2 v^2 \sigma l A \tag{2.3.7}$$

The experiments for the evaluation of power output are carried out considering highway excitation and the RMS voltage measured is $9.30\,V$. The performance of a full scale regenerative shock absorber is estimated as $16 - -64\,W$. This is the total power that could potentially be harvested, but the actual power will also depend on the harvesting power electronics.

2.3.3 Hydraulic pumping damper devices

These devices consist of an energy recovery unit and a hydraulic actuator. They can harvest energy from suspension vibration, and in addition, can achieve a variable damping force by controlling the electrical load of the energy recovery unit [8]. The complete system consists of a hydraulic pump, a DC generator, an accumulator, two check valves and a regenerative circuit. During the extension/compression phases, the oil flows through the hydraulic pump that, in turn, drives the DC motor to generate electric power. The scheme of the damper is shown in Figure 2.6.

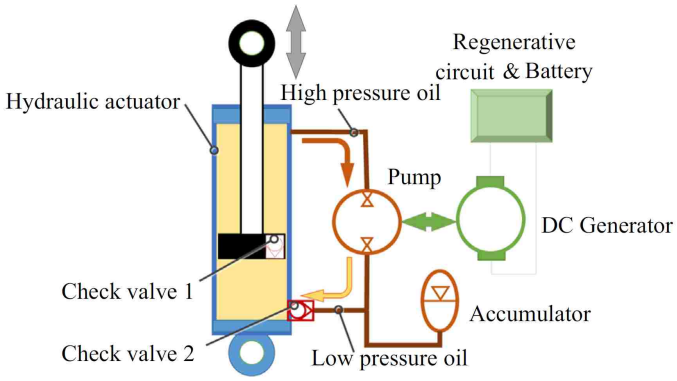

Figure 2.6: *Scheme of hydraulic pumping damper (figure reproduced from [13])*

The regenerative hydraulic damper is capable of recovering mechanical energy coming from vibration. The use of the hydraulic motor amplifies the transmission between vibratory excitation and power generation. The displacement of the piston makes the oil flow from

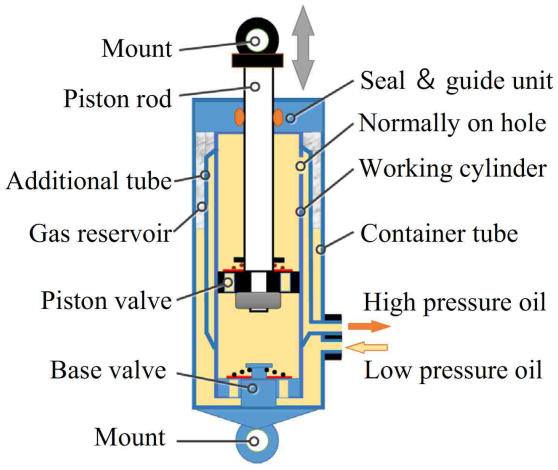

Figure 2.7: *Overall structure of an integrated hydraulic actuator (figure reproduced from [13])*

one chamber to the other, passing through the hydraulic motor. According to the theory of back electromotive force, the damping forces can be adjusted by changing the generator external circuit load, as in Figure 2.8. Y. Zhang *et al.* [13] proposed a mathematical model

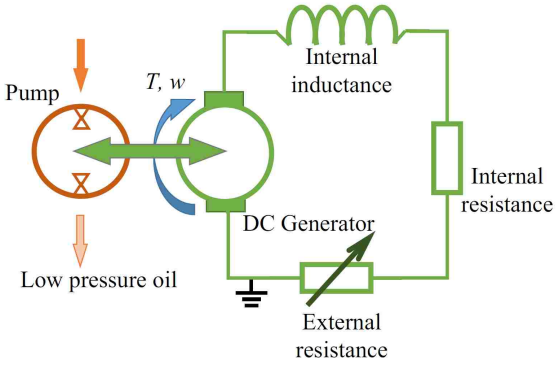

Figure 2.8: *Energy recovery unit model (figure reproduced from [13])*

of this regenerative suspension system, and then the damping characteristic, regenerative power and regenerative efficiency of different hydraulic pumping regenerative suspension structures are studied under different input frequencies and electrical loads. The energy recovery part of the mathematical model is based on the following equations. When the high pressure oil drives the hydraulic pump, its rotation speed ω and output torque T_{pump}

are given by

$$\omega = \frac{2\pi Q_{pump}}{q}\eta_v \tag{2.3.8}$$

$$T_{pump} = \frac{\Delta P_{pump} q}{2\pi}\eta_m \tag{2.3.9}$$

where Q_{pump} is the flow rate through the pump, q the pump capacity, ΔP_{pump} the pressure drop, η_v and η_m are the volumetric and mechanical efficiencies. Several studies on the behavior of the damper were carried out, in particular considering the effect of the electric circuit linked with the damper itself. In Figure 2.9, the behavior of the damper considering different electrical loads is shown. The plot shows that a damping force range from

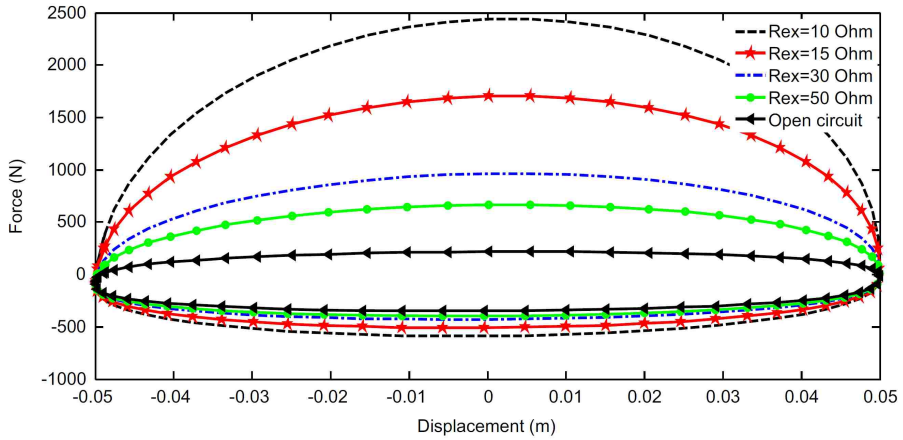

Figure 2.9: *Force-displacement loops with different electrical loads (figure reproduced from [13])*

250 N to 2400 N can be obtained by adjusting the external electrical load, which brings a large changeability. Concerning the efficiency, with a constant external load of 15 Ω, a considerable electrical efficiency and a 73.2% hydraulic efficiency can be achieved.

2.3.4 Magneto-rheological dampers

Magneto-rheological (MR) dampers are semi-active control devices using MR fluids. These fluids have the characteristic that, when subjected to an external magnetic field, they change their rheological properties. When subjected to magnetic field, the particles acquire a dipole moment that causes them to create linear chains parallel to the imposed magnetic field [15]. These devices need a power supply to generate the magnetic field. However, self-powered MR dampers have been studied [16]. This damper is composed of the MR damper part, the

power generator, interaction components and mounting and motion guidance components. To reduce the size of the damper, the power generator is concentric and radially outside the MR damper. The power generator is used both for power generation and velocity sensing. The excitation frequencies that could be reached by MR dampers in their application are quite low. For this reason, in order to have a high conversion efficiency a linear multi-pole electromagnetic generator is used for power generation. Zheng *et al.* [29] conducted studies

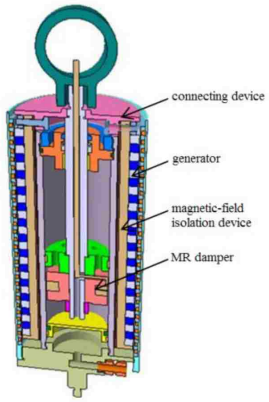

Figure 2.10: *Self-powered MR damper (figure reproduced from [16])*

on the integration of a permanent magnet linear generator in an MR damper in order to achieve energy harvesting from a vehicle suspension system. The MR damper in this paper has two functions: vibration isolation and energy harvesting. It is composed of an MR damper, magnetic field isolation, connecting device, and energy harvester. The linear electromagnetic generator is concentric with the MR damper. The interaction components include the guide rail, flux guide and flux shield layers. During the motion of the damper, the relative movement between mover and stator of the linear electromagnetic generator happens. Moreover, the yield strength of MR fluid can be controlled by adjusting the input current to the MR damper, thus producing the controllable damping force.

2.3.5 Ball-screw dampers

This electro-mechanical actuator consists of a DC motor and a ball screw mechanism. It converts the linear motion of vibration into input torque for a motor. In passive use, the electro-mechanical actuator uses electro-mechanical force as damping force and the damping

force can be electrically controlled by the induced current [23]. This actuator has several important characteristics:

- High controllability achieved by tunable damping force
- Active suspension
- Energy regeneration

The output force, F_d, is evaluated as:

$$F_d = \Phi i - I_d \ddot{z} - f_r \operatorname{sgn} \dot{z} \tag{2.3.10}$$

where f_r is dynamic friction coefficient and I_d the equivalent inertia in equation 2.3.11.

$$I_d = \left(\frac{2\pi}{l_b}\right)^2 J \tag{2.3.11}$$

where l_b is the lead of the ball screw and J is the moment of inertia of the motor rotor and ball screw. A voltage is applied to the motor in order to generate control input according to Equation 2.3.12.

$$u = -C_s \dot{x}_s - C_u \dot{x}_u \tag{2.3.12}$$

where $\dot{x}_s$ and $\dot{x}_u$ are, respectively, the velocity of sprung and unsprung mass, and C_s and C_u are the velocity feedback gain of the sprung and unsprung mass. According to experiments done by Kawamoto *et al.* [23] under conditions of a vehicle traveling at $80\,km/h$ on the rough road equivalent to C level of ISO standard, energy is consumed to isolate the vibration mode of the sprung mass below about $2\,Hz$. Above this value, energy is regenerated. Huang *et al.* [30] proposed a new adaptive suspension system based on ball screw mechanism. The function of the ball screw is to control the nut position through the balls rolling between the screw and nut. In this study, if it is given that screw rotation is input, nut displacement is output, as shown in Figure 2.11. The motion of the ball screw can be derived as

$$Z_r - Z_s = Z_L \tag{2.3.13}$$

where Z_L is the vertical displacement of the vehicle, Z_r the road surface change and Z_s the suspension supplement displacement. The schematic of the controller is shown in Figure

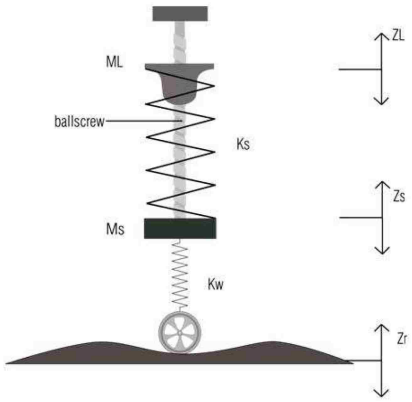

Figure 2.11: *Ball screw mechanism of vehicle suspension (figure reproduced from [30])*

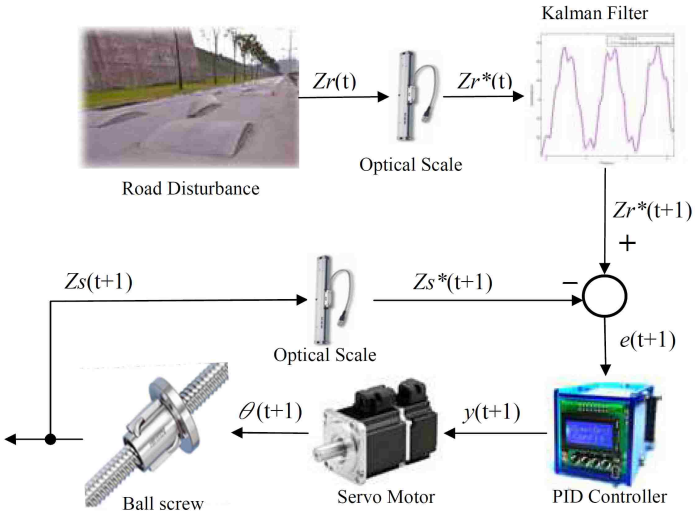

Figure 2.12: *Controller for ball screw damper (figure reproduced from [30])*

2.12. In this system the road disturbance $Z_r(t)$ as well as the surface variation is measured via optical scales. Next, in order to overcome time delay problem,the Kalman filter is used to estimate the road condition $Z_r(t+1)$. Then, after the comparison between the estimated result and the ball screw supplement is made, an error signal $e(t+1)$ will yield the input of a PID controller. Then, according to the above error signal, the PID controller calculates the error supplement $y(t+1)$ to position the ball screw via the motor. Finally, the suspension supplement $Z_s(t+1)$ resulting from the ball screw will be given as feedback to yield a new error signal for the next step. Other studies on ball-screw regenerative dampers were carried out by Huang *et al.* [28]. The configuration of the quarter car is, in this case, the one shown

in Figure 2.13. The system is made up of a mass-spring-damper system and a switch-mode

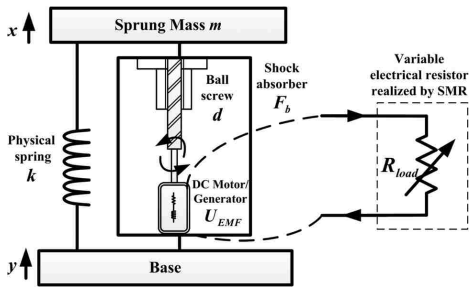

Figure 2.13: *1-DOF* quarter car model with ball-screw regenerative damper (figure reproduced from [28])

rectifier (SMR) connected to the terminals of the DC motor. It is demonstrated that the output force generated by the damper can be computed according to equation 2.3.14.

$$F_d = \frac{k_e k_t k_g^2 \eta_g^2}{(R_{int} + R_{load}) d^2 \eta_b^2} \dot{z} + \frac{J_m k_g^2 \eta_g^2 + J_g + J_b}{d^2 \eta_b^2} \ddot{z} \tag{2.3.14}$$

where $d = l/2\pi$ and $z = x - y$. J_m is the inertia of the motor, J_g the one of the gearbox, J_b the one of the ball screw. The gearbox and ball screw efficiencies are η_g and η_b, respectively. The force generated by the damper is dependent on the external resistance, which in this case is also a control parameter.

2.3.6 Rack and pinion dampers

The rack and pinion mechanism can convert linear motion into rotation. Suda *et al.* [24] studied a regenerative active suspension combining a rack and pinion and a rotary motor. Beno *et al.* [25],[26] developed an electronically controlled active suspension system that adopted the rack and pinion configuration. The experimental results indicated that the limit speed and handling performance of vehicle had been enhanced significantly. Zhongje Li *et al.* [31] presented the design, modeling, bench experiments, and road tests for a retrofit regenerative shock absorber based on a permanent magnetic generator and a rack-pinion mechanism for energy harvesting and vibration damping. The shock absorber model is shown in Figure 2.14. The shock absorber has several parts, including a generator, a planetary gearbox, bevel gears, rack and pinion, etc. The prototype is then evaluated on a testing machine with sinusoidal displacement inputs. The results show that the equivalent

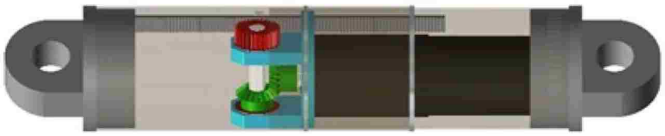

Figure 2.14: *Model of rack-pinion shock absorber (figure reproduced from [31])*

damping coefficient depends on the external electrical resistance. The selection of gears is critical for the overall performance. With a high transmission ratio, the system can achieve a higher damping coefficient, but it also means a low transmission efficiency. The selection of gears is a compromise between performance, efficiency and compactness. A critical aspect of this damper is the bevel and rack and pinion gears that may cause failure. For this reason, contact fatigue, and the strength of the teeth surface and root should be checked. It is demonstrated in [31] that the equivalent damping ratio of this shock absorber is given by Equation 2.3.15.

$$C_{eq} = \frac{k_g^2 k_e k_t}{r^2 \eta_g R} + k_v \tag{2.3.15}$$

where k_g is transmission ratio from the pinion gear to the generator rotor, k_e is the voltage constant, k_t is the torque constant, r the pinion radius, η_g the gear transmission efficiency, $R = r_i + R_e$ the loop resistance and k_v the viscous friction coefficient between the inner and outer cylinders. It is evident that the external resistance R_e is an important parameter for the damping coefficient and, for this reason, a control parameter. A total energy conversion efficiency of up to 56% was achieved. During road testing, a peak power of $67.5\,W$ was achieved with a vehicle velocity of $48\,km/h$ on a fairly smooth test road.

2.4 Control strategies

By knowing the amount of force the damper is capable of producing and using key attributes of the suspension system (typically the velocities of the sprung and unsprung masses) an optimal amount of damping force can be produced to meet the objective of the system (road-holding, comfort or a combination of both). In order to achieve this functionality, a control algorithm or strategy must be implemented. A variety of control algorithms have been developed over the years and an extensive amount of literature is available for semi-

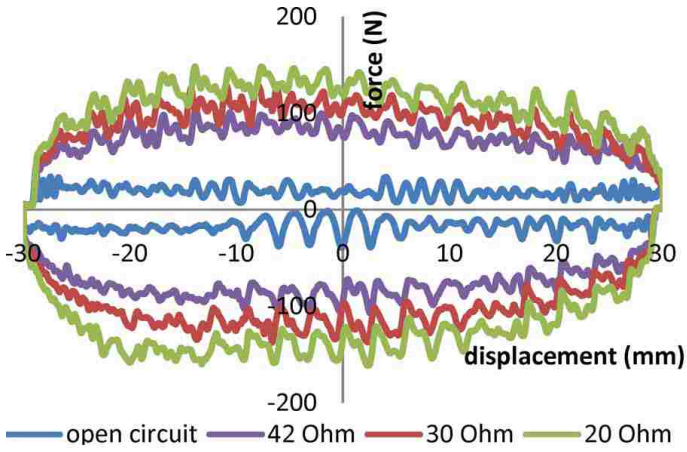

Figure 2.15: *Force-displacement loops for different electrical loads at displacement input of* $0.1\,Hz$ *frequency and* $30\,mm$ *amplitude obtained with rack-pinion regenerative damper (figure reproduced from [31])*

active and fully-active systems. In both semi-active and fully-active configurations, the most commonly applied control strategies are Skyhook and Groundhook.

2.4.1 Skyhook control

The Skyhook control technique was first developed by D. Karnopp *et al.* [36]. This control strategy is typically associated with comfort rather than road-holding. In order to achieve the comfort objective, the algorithm attempts to minimize the amount of displacement experienced by the sprung mass in a typical quarter-car model. The physical model for this control strategy consists of a damping element connected between a sky reference frame (above the suspended mass) and the suspended mass, a spring element between sprung and unsprung mass and a secondary spring element between unsprung mass and the road reference frame. Equation 2.4.1 reflects how the damping coefficient would vary in an on/off or two state configuration as a function of the velocity of the suspended and unsprung mass masses respectively.

$$c = \begin{cases} -c_{max} & \text{if } \dot{z}_M(\dot{z}_M - \dot{z}_m) \geq 0 \\ c_{max} & \text{if } \dot{z}_M(\dot{z}_M - \dot{z}_m) < 0 \end{cases} \tag{2.4.1}$$

In the above mentioned equation, c represents the damping coefficient returned by the algorithm, $\pm c_{max}$ represents the maximum damping coefficient the damper is capable of

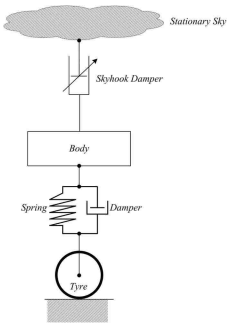

Figure 2.16: *Skyhook control scheme (figure reproduced from [32])*

producing in the positive and negative direction, and $\dot{z}_M$ and $\dot{z}_m$ represent the velocities of the suspended and unsprung mass respectively. The logic behind this equation is only applicable to a fully-active system, because of semi-active dampers' inability to produce an active force. For this latter kind of damper, the expression $+c_{max}$ would be zero or the steady state value of the damper.

2.4.2 Groundhook control

The objective of the Groundhook control strategy is road-holding, as oppose to comfort seen in the Skyhook model. The Groundhook control strategy was first developed by Valek *et al.* [37] and the basis of the model is to reduce tire force fluctuation and deflection of the unsprung mass. The physical model used for this control strategy consists of a spring element between the suspended and unsprung masses, a secondary spring element between the unsprung mass and the road reference frame, and a damping element between the unsprung mass and a ground reference frame below the road reference. Equation 2.4.2 reflects the logic used in the Groundhook control strategy based on a two state configuration.

$$c = \begin{cases} -c_{max} & \text{if } \dot{z}_m(\dot{z}_M - \dot{z}_m) \geq 0 \\ c_{max} & \text{if } \dot{z}_m(\dot{z}_M - \dot{z}_m) < 0 \end{cases} \tag{2.4.2}$$

All the variables are the same as shown in the Skyhook control section.

2.5 Electrical circuit for energy recovery

The electricity recovered by the shock absorber can be used to charge the battery. In this way, the alternator does not have to produce that amount of electricity, in the case of conventional ICE vehicle. In the case of electric or hybrid vehicles, the energy can be directly used as a power source. Depending on the technology used, the current generated could be alternating (AC) or direct (DC). In the case of AC type, a rectifier is needed, and associated power losses must be taken into account. Even if DC current is obtained as output, a dedicated DC/DC converter has to be used to adapt the voltage coming from the harvester output to the one of the battery. Typical values of efficiency for electrical converters are in the range $92 - -94\%$.

2.5.1 DC motor and DC generator working modes

Permanent magnetic DC motors can be directly used as generators. To analyze the two working modes, the two circuits in Figure 2.17 are considered. When the electrical machine

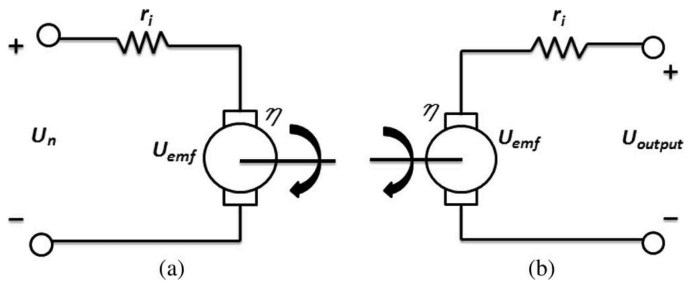

Figure 2.17: *Two working modes of electrical machines. a) As a motor. b) As a generator (figure reproduced from [31])*

of internal resistance r_i is used as a motor, the relationship between the input voltage U_n and back electromotive force voltage U_{emf} at nominal current I_n is

$$U_n = I_n r_i + U_{emf} \tag{2.5.1}$$

Furthermore, when it is used as generator, the output voltage U_{output} at nominal current I_n is

$$U_{emf} = I_n r_i + U_{output} \tag{2.5.2}$$

where the back EMF voltage is proportional to rotation speed ω_n with gain k_e of the back electromotive voltage constant. Equations 2.5.1 and 2.5.2, when the motor is used as a generator, at the same nominal speed and current, the output voltage U_{output} may be much smaller than the nominal input voltage U_n of the motor.

2.5.2 Buck-boost converter for damping control

A buck-boost converter is a type of switching DC-DC converter that can either increase or decrease the magnitude of the input voltage. The schematic of a buck-boost converter is shown in Figure 2.18. When the buck-boost converter works in discontinuous conduction

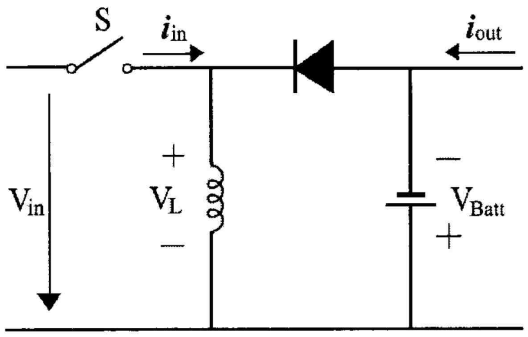

Figure 2.18: *Schematic of buck-boost converter with ideal inductor (figure reproduced from [33])*

mode, the equivalent input resistance is only related to the duty cycle D, and the relationship between the R_{in} and D is

$$R_{in} = \frac{2Lf_{sw}}{D^2} \tag{2.5.3}$$

where f_{sw} is the switching frequency and L is the inductance. Because the current and voltage in a switching converter is always oscillating in a small range due to the switching, the ratio is averaged over a reasonable period of time [33]. The condition for the converter to work in DCM is related to the range of input voltage and the battery voltage connected to the output of the buck boost converter, and duty cycle D. The conditions are:

$$V_{in} < \frac{1-D}{D} V_{battery} \tag{2.5.4}$$

$$D < \frac{V_{battery}}{V_{battery} + V_{in}} \tag{2.5.5}$$

The different parameters can be designed or controlled to meet the condition of DCM and at the same time achieve the desired damping range.

2.6 Remarks on vehicle dynamics

When talking about vehicle dynamics, the analysis is generally divided into three domains. When the investigation is focused on the vehicle's longitudinal direction, it is referred to as *longitudinal dynamics*. The objects of interest in longitudinal dynamics are mainly the vehicle's driving resistance and power, as well as braking and traction properties. The second domain is *lateral dynamics*, i.e., the dynamics in the direction transverse to the longitudinal one. The main concern here is about the motions affecting dynamic stability, cornering and road holding. The last domain is *vertical dynamics*, concerned with vehicle motion in vertical direction [6].

2.6.1 Longitudinal dynamics

When a car is parked on a level ground the normal force, F_z due to the weight of the car is not always equally distributed between the front and rear axle. In fact, it depends on the position of the center of gravity of the car and, in particular, indicating with the subscript 1 the front axle and with 2, the forces are:

$$F_{z1} = mg\frac{b}{l} \tag{2.6.1}$$

$$F_{z2} = mg\frac{a}{l} \tag{2.6.2}$$

where a is the distance between the center of gravity and the front axle, b the one from the center of gravity to the rear axle and l is the wheelbase. During events of braking or acceleration, there is a load transfer between front and rear axles. The new forces on the two axles are:

$$F_{z1} = \frac{m}{l}\left(gb - h\frac{dV}{dt}\right) \tag{2.6.3}$$

$$F_{z2} = \frac{m}{l}\left(ga + h\frac{dV}{dt}\right) \tag{2.6.4}$$

where h is the height of the center of mass.

Acceleration and braking During acceleration and braking, external forces act on the vehicle. During the braking phase, the vehicle's effective inertia force acts at its center of gravity

$$F_i = -ma_x \tag{2.6.5}$$

Since the acceleration has negative value, the force points in the direction of vehicle travel. This force is equal to the sum of the longitudinal braking forces exchanged between the wheels and the ground. Also, forces in the vertical direction arise, both in front and rear axles, but with opposite direction, thus creating a pitching moment. The same analysis holds for the acceleration condition. The difference in this case is that the inertia force point in the direction opposite to the one of travel and the load transfer on front and rear axles has opposite direction as well.

2.6.2 Vertical dynamics

Vertical forces can arise from several factors such as uneven roads, load transfer during pitch or roll conditions, and also internal excitation due to the powertrain. These forces can create disturbances that reduce ride comfort. The suspension system has the goal to reduce the vehicle body accelerations and reduce roll and pitch motions as well as load transfer. These forces are caused by the spring and the damper components.

Road irregularities Road profiles are usually rather complex, also involving concentrated obstacles, such as bumps or potholes. The main frequency content of these excitation is usually below $200 - -300\,Hz$ depending on vehicle speed [19]. The main design parameters to reduce the vibrations caused by these irregularities are the ones of the vehicle suspension. The road surface is never completely flat, but irregularities of different shape, amplitude and distribution are always present. These irregularities are characterized by measuring the vertical road profile z as function of the travel distance d. From experimental measurements of the road profile, a law can be defined and its power spectral density can be obtained with harmonic analysis. The profile is a function of space, and the spatial frequency ν is measured in $cycles/m$. The power spectral density is thus measured in

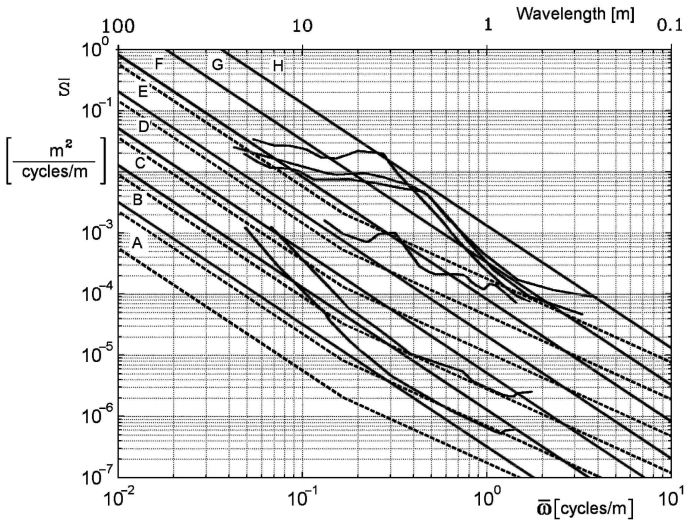

Figure 2.19: *Power spectral density of road profiles (figure reproduced from [17])*

$m^2/(cycles/m)$ and is computed according to the law

$$\bar{S} = c\bar{\nu^{-N}} \tag{2.6.6}$$

The International Organization for Standardization (ISO) subdivides the road profiles into eight different classes, indicated with letters from A to H, with different values for the c coefficient. The previous expression can be written as function of time. In case the vehicle is travelling with velocity V, the Power Spectral Density (PSD) becomes

$$S = cV^{N-1}\nu^{-N} \tag{2.6.7}$$

So ISO has proposed road roughness classification using the PSD. Paved roads are generally considered to be among road classes A to D. The PSDs of roads show a characteristic drop in magnitude with the wave number. In Table 2.1, the values of constant c for all road classes are given. To generate a random road profile, Lei Zuo and Zhang [8] used a white noise input through a first order filter. When a vehicle is thus driven at speed V, the temporal excitation frequency ω and the spatial frequency ν are related by $\omega = 2\pi V\nu$ and $S_{PSD}(\omega)d\omega = S_{PSD}(\nu)d\nu$. The power spectral density of road excitation in terms of temporal frequency can be obtained as

$$S_{PSD}(\omega) = \frac{2\pi G_r V}{\omega^2 + \omega_0^2} \tag{2.6.8}$$

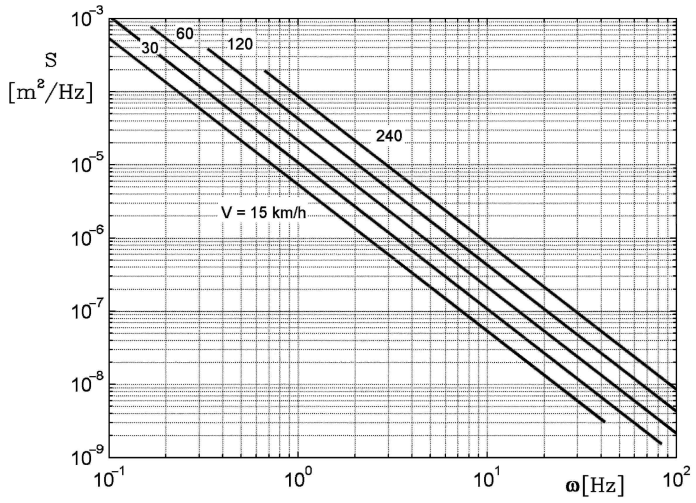

Figure 2.20: *Power spectral density of the displacement as a function of the frequency ω at various speeds for road at the border between the B and C classes (figure reproduced from [17])*

where G_r is the road roughness coefficient and ω_0 is a small cutoff frequency added to limit the displacement to be finite at vanishingly small spectral frequencies. Therefore, this displacement disturbance can be represented by a unit-insety white noise signal $w(t)$ passing through a first-order filter given by

$$G(s) = \frac{2\pi\sqrt{G_r V}}{s + \omega_0} \tag{2.6.9}$$

and being ω_0 very small, it indicates that the ground velocity input is a white noise with intensity of $2\pi\sqrt{G_r V}$, which is proportional to the road roughness coefficient G_r and vehicle driving speed V.

Effect of vibrations on human body The ability of the human body to withstand vibration and related discomfort has been the object of numerous studies and several standards have been stated. The ISO 2631 [34] distinguishes between vibrations with a frequency range of $0.5 - -80\,Hz$ that may cause a reduction of comfort, fatigue, and health problems, and vibrations with a frequency range of $0.1 - -0.5\,Hz$ that may cause motion sickness. Standards refer to the acceleration due to vibration and suggest weighting functions of the frequency to compute the root mean square values of the acceleration. Such functions depend both on the point of the body where the acceleration is applied and the direction

Class	c_{min} $(m^2 cycles/m)$	c_{avg} $(m^2 cycles/m)$	c_{max} $(m^2 cycles/m)$
A	–	$1.6 \cdot 10^{-7}$	$3.2 \cdot 10^{-7}$
B	$3.2 \cdot 10^{-7}$	$6.4 \cdot 10^{-7}$	$1.28 \cdot 10^{-6}$
C	$1.28 \cdot 10^{-6}$	$2.56 \cdot 10^{-6}$	$5.12 \cdot 10^{-6}$
D	$5.12 \cdot 10^{-6}$	$1.024 \cdot 10^{-5}$	$2.048 \cdot 10^{-5}$
E	$2.048 \cdot 10^{-5}$	$4.096 \cdot 10^{-5}$	$8.192 \cdot 10^{-5}$
F	$8.192 \cdot 10^{-5}$	$1.6384 \cdot 10^{-4}$	$3.2768 \cdot 10^{-4}$
G	$3.2768 \cdot 10^{-4}$	$6.5536 \cdot 10^{-4}$	$1.31072 \cdot 10^{-3}$
H	$1.31072 \cdot 10^{-3}$	$2.62144 \cdot 10^{-3}$	–

Table 2.1: *Minimum, average and maximum value of constant c for each road class according to ISO 8606*

along which it acts. Figure 2.21 shows the root mean square value of acceleration causing, in a given time, a reduction of physical efficiency.

2.6.3 Lateral dynamics

In the case of lateral dynamics, the driver is responsible in regulating the vehicle behavior in the lateral direction. In general, there are disturbances acting both on the vehicle and on the driver. These disturbances are overcome by the driver regulating different parameters, e.g., the steering wheel angle. For this reason, the properties of the vehicle play a major role in determining whether the vehicle-driver system behavior will remain stable during the manoeuvres necessary during driving.

2.7 Vehicle usage statistics

In this section, the statistics concerning the annual average vehicle usage are shown. This is done to evaluate after the simulation the real benefits in terms of energy recovery during the whole lifetime of the vehicle. When we consider the usage statistics in North America, from

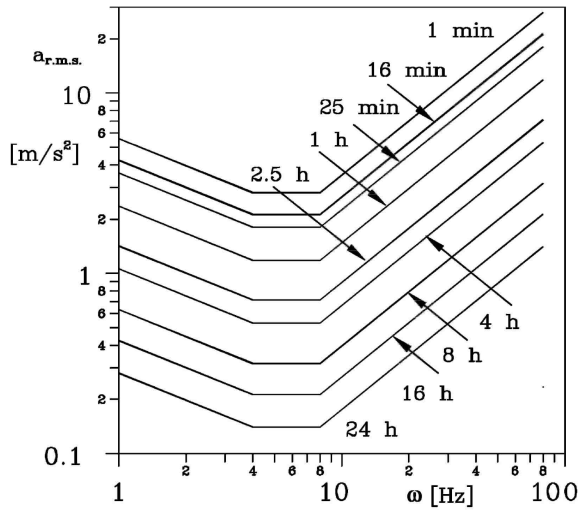

Figure 2.21: *RMS value of the vertical acceleration causing reduced physical efficiency (figure reproduced from [17])*

the U.S. Department of Transportation (DOT) [35], the average mileage is done according to different categories:

- typology of road (highway or urban)
- typology of driver (divided according to gender and age)

The results of the past year are shown in Table 2.2. When considering all the categories,

Table 2.2: *Annual miles per driver by age group*

Age	**Male**	**Female**
16-19	8206	6873
20-34	17976	12004
35-54	18858	11464
55-64	15859	7780
65+	10304	4785

on average 13476 miles per year are traveled, i.e. 21687 kilometers per year. Moreover, according to the DOT, about the 55% of this mileage is on highways, and the remaining 45% in the urban environment.

Chapter 3

Model description

In this chapter the modeling techniques employed to generate and analyze the regenerative suspension system together with the full vehicle model are developed and discussed. The full-vehicle model is the one of a segment C car, the Alfa Romeo Giulietta, created with CarSim®. This model contains all the information of the real car, including the suspension system, that has a regular passive damper. The model of the regenerative damper is instead a Simulink® one, so an integration between the two software environments is necessary. The modeling strategy adopted is composed by different steps:

1. Analysis of the CarSim vehicle model.
2. Analysis of the CarSim vehicle model with passive dampers integrated in the Simulink environment and correlation of the second model with the original one.
3. Evaluation of ideally recoverable energy from the passive damper.
4. Analysis of the vehicle sprung mass accelerations with passive damper.
5. Creation of the CarSim model with the regenerative damper.
6. Tuning of regenerative damper to achieve good energy harvesting performances in conjunction with ride comfort and road handling.

7. Analysis of the vehicle sprung mass accelerations with regenerative dampers and comparison with the passive ones.

8. Evaluation of CO_2 savings according to the electrical power generated by the damper, that must not be provided by the alternator.

After the completion of all these steps, the results obtained in each configuration will be analyzed and discussed. In the following sections each step will be described in detail.

3.1 Full car model

As already mentioned in the brief chapter introduction, the model of the car on which the regenerative dampers will be applied is an Alfa Romeo Giulietta (denoted as a segment C). Some general technical specifications of the car, such as dimensions are reported in

Figure 3.1: *Vehicle used in all the simulations of this work*

Table 3.1. However, the most important feature in relation to the current research is the suspension system, in particular the damper component. From the model, the front and rear dampers show different characteristic curves. The plots in Figure 3.2 show the force vs velocity curves of the front and rear dampers. The next step is the implementation of these characteristic curves inside the Simulink environment, in order to separate the damper from the CarSim model. This step will be analyzed in the following section.

Table 3.1: *Dimensions of the examined car*

Quantity	Unit	Value
Length	mm	4350
Width	mm	1800
Height	mm	1470
Wheelbase	mm	2634
Weight	kg	1320

3.2 Damper implementation in Simulink environment

In order to have the damper component separated from the CarSim model, it must properly be characterized in the Simulink environment. To accomplish this operation the *1-D lookup table* function has been used. This function performs an n-dimensional interpolated table including search index. In this way, the table represents a sampled representation of the damper characteristic. In order to make these tables work, the velocity inputs coming from the dampers of the CarSim model are necessary. These inputs will be sent to the first port of the look-up table, and as an output the damper force corresponding to the velocity abscissa value is provided. The CarSim model, in order to accomplish the above mentioned operation, is sent to Simulink as an S-function from which the velocity output are provided and accordingly the force inputs are computed and sent back to the vehicle S-function. In Table 3.2 the inputs and outputs of the S-function are described. The final model considering all the inputs and outputs in the table is shown in Figure 3.3. On the right, it is possible to notice all the outputs of the vehicle S-function. The top four outputs are the damper compression rates, the gains are used for unit conversion purposes (the outputs of the S-function are in mm/s while the inputs of the look-up tables are in m/s). Also the characteristic angles and accelerations of the vehicle are given as outputs and sent to the Matlab®workspace in order to be able to compare the results obtained from these simulations to those of the original model.

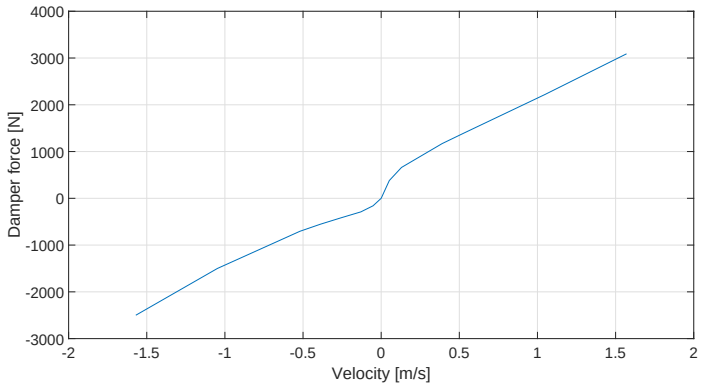

(a) *Passive front damper force-velocity characteristic*

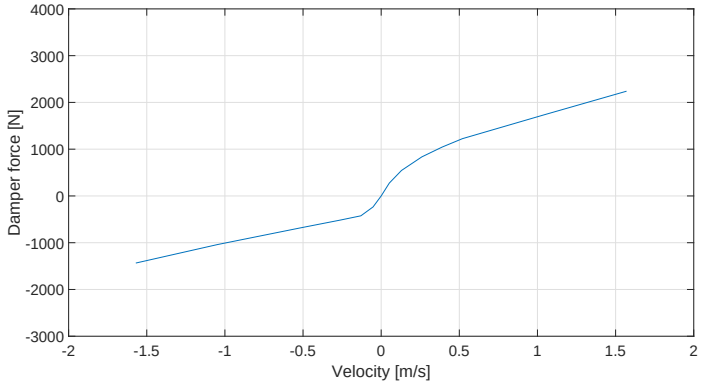

(b) *Passive rear damper force-velocity characteristic*

Figure 3.2: *Damper characteristics*

3.2.1 Validation on original model data

To check the correlation between the two models, several tests have been conducted. The model was tested according to different procedures, in particular the *double lane change* and *sine sweep* test. A brief explanation of the two tests follows.

3.2.2 Double lane change

As regulated by the ISO 3888 standard, where it is called the ISO lane-change test, this test is widely used to evaluate handling and its key components. The specification defines the position of a series of cones through which the vehicle must be safely driven. The width of the lane depends on the vehicle dimensions. The complete path is shown in detail in Figure

Table 3.2: *Input/Output variables of vehicle S-function*

	Variable	Unit	Description
Inputs	FD_L1	N	Damper force, left side, axle 1
	FD_L2	N	Damper force, left side, axle 2
	FD_R1	N	Damper force, right side, axle 1
	FD_R2	N	Damper force, right side, axle 2
Outputs	$CmpRD\_L1$	mm/s	Damper compression rate, left side, axle 1
	$CmpRD\_L2$	mm/s	Damper compression rate, left side, axle 2
	$CmpRD\_R1$	mm/s	Damper compression rate, right side, axle 1
	$CmpRD\_R2$	mm/s	Damper compression rate, right side, axle 2
	Pitch	deg	Pitch angle
	Roll	deg	Roll angle
	Yaw	deg	Yaw angle
	A_z	$g's$	Vertical component of acceleration
	A_y	$g's$	Lateral component of acceleration
	A_x	$g's$	Longitudinal component of acceleration

3.4. To begin this maneuver, the vehicle is driven in a straight line at a desired entrance speed. Two meters after the start of the entry lane the throttle is released so that the entire maneuver is completed in the overrun mode with the top gear and an engine speed of at least 2000 rev/min. No throttle input or brake application is permitted during the remainder of the maneuver [38].

3.2.3 Vertical sine sweep test

This test is used to evaluate the chassis behavior under different kinds of amplitude and frequency excitations. During the test, the amplitude of the road excitation is decreased while the frequency is increased. The elevation of the road is shown in Figure 3.5.

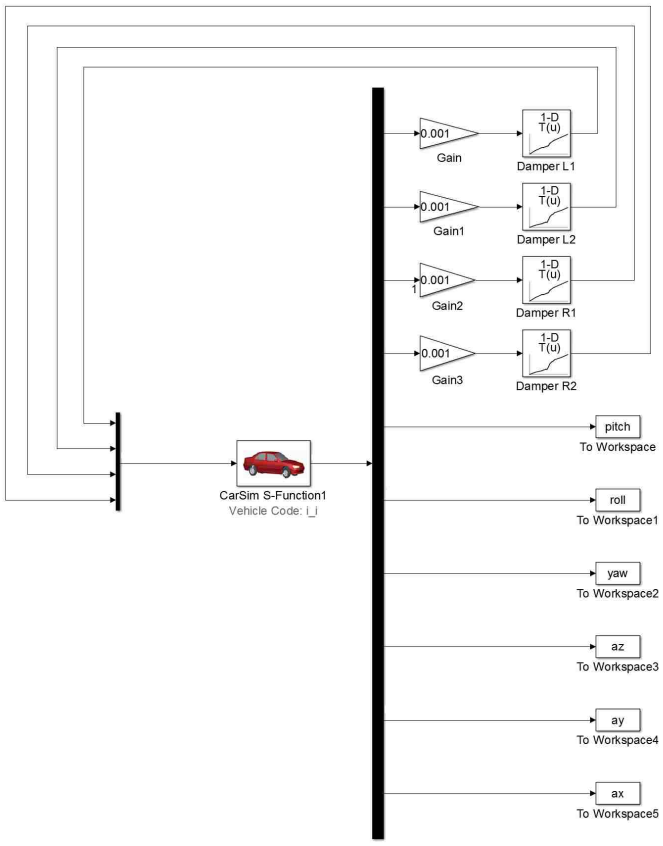

Figure 3.3: *CarSim and Simulink model with passive dampers*

3.2.4 Evaluation of the results

The same tests have been used in both the original and the modified model. The same outputs have been collected for correlation purposes. The correlation quantification has been done according to the correlation metric proposed by Oberkampf and Trucano [39]. This correlation metric has the following features:

- it incorporates an estimate of the numerical error in the simulation;
- the results reflect all uncertainties and errors incurred in the modeling and simulation;
- in case of experimental parameters, the metric is able to incorporate uncertainty in the computation that is due to both random uncertainty in experimental parameters and any uncertainty that is due to the lack of experimental measurement of needed computational quantities.

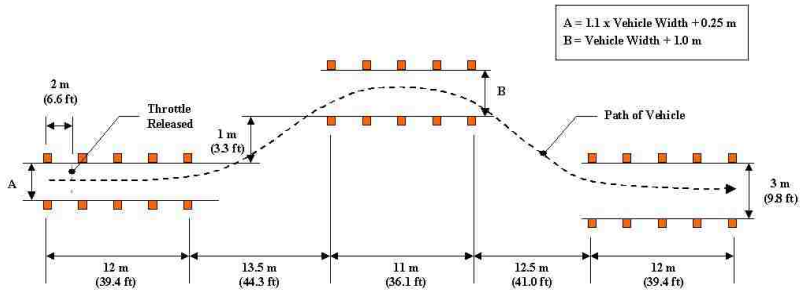

Figure 3.4: *ISO 3888 lane-change test (figure reproduced from [5])*

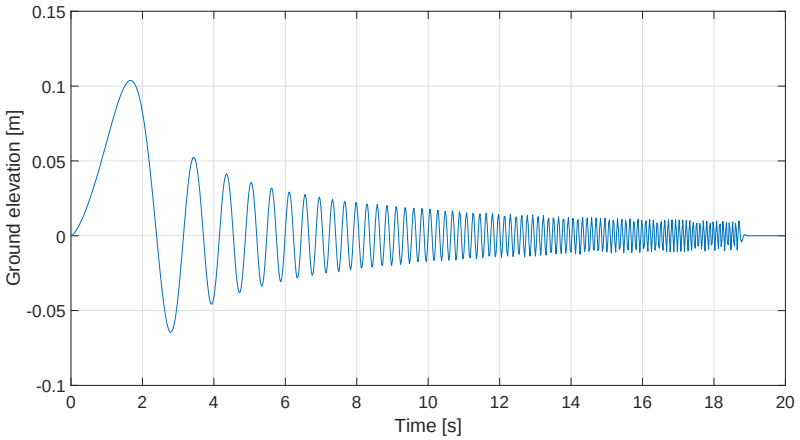

Figure 3.5: *Sine sweep test - ground elevation profile*

The mathematical expression of the correlation metric is given by equation 3.2.1.

$$V_m = 1 - \frac{1}{t_{end} - t_0} \int_{t_0}^{t_{end}} \tanh \left| \frac{y(t) - Y(t)}{Y(t)} \right| dt \tag{3.2.1}$$

Where V_m is the correlation metric, $y(t)$ the value obtained by the model that must be validated, and $Y(t)$ the theoretical value obtained by the original model. This type of metric has the following advantages:

- it normalizes the difference between the simulation data and the theoretical ones. Thus a relative error norm is computed;
- the absolute value of the relative error only permits difference between the two values to accumulate, i.e. positive and negative differences cannot offset one another;
- when the difference between the values is zero, then the correlation metric is exactly equal to unity;

- when the summation of the relative errors becomes large, the correlation metric approaches zero.

After all the simulations, all the data necessary for the correlation are recorded and then analyzed. Some of the quantities are shown in Figure 3.5. The quantities obtained with the original model are shown on the left, the ones obtained with the modified Simulink model are on the right. These plots are some of the results coming from the simulation of the double lane change and sine sweep tests. As it can be graphically noticed, the fitting of the data is very good. Very small discrepancies can be seen only when near the presence of sharp peaks of the analyzed quantity. In particular, a small difference is quite evident in the first peak of the vertical acceleration, however it is a negligible gap. To go further in the evaluation of the model capabilities, it is necessary to quantify how good is the fitting of the curve. To do this, the plot data have been exported to the Matlab®environment. Since the simulations of the original model and the modified one have different time-steps, the correspondence is not perfect between the two vectors of data. For this reason an interpolation of one of the datasets is necessary. To achieve a good result in interpolating the values, the `fit` function was used with a *cubic spline* interpolation. After this step, the evaluation of the error and correlation metric is possible according to Equation 3.2.1. The same procedure has also been used for the data collected with the sine sweep test. For sake of brevity, not all the data collected are plotted here and the results of the correlation metric are shown in Table 3.3 (the complete data are available in Appendix A). As expected

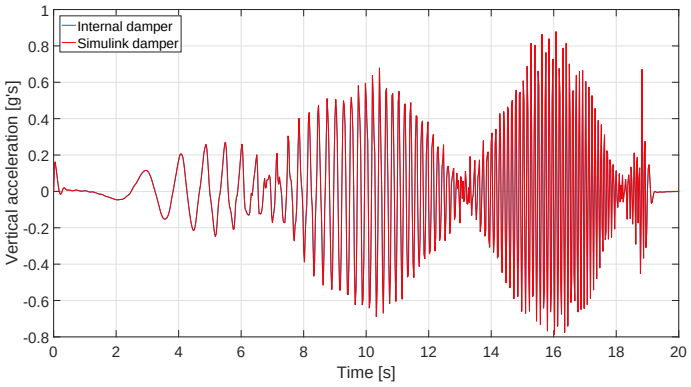

(a) *Vertical acceleration - Original model (sine sweep test)*

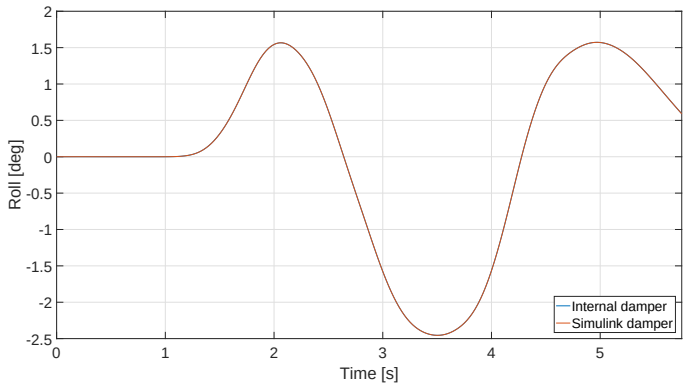

(b) *Roll angle - Original and modified model (double lane change)*

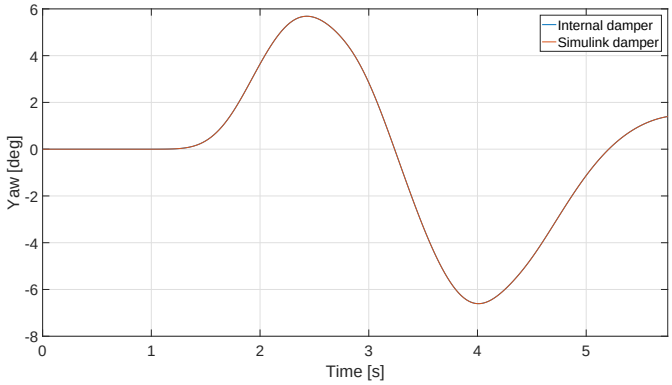

(c) *Yaw angle - Original and modified model (double lane change)*

Figure 3.5: *Model outputs*

from the graphical analysis the results are within 2.4% of 100%, thus indicating a very good fit between the original CarSim®model and the modified in Simulink®one. Now that the model has been correlated to the original , it is possible to go to the next step, i.e. the evaluation of the dissipated power at the damper level that is also the power that could be harvested by an ideal energy recovery system. In the next section, the model to evaluate the dissipated power will be created and the generation of the road profiles will also be addressed.

Table 3.3: *Validation results for all quantities*

	Longitudinal acceleration	**Lateral Acceleration**	**Vertical Acceleration**	**Roll angle**	**Pitch angle**	**Yaw angle**
Validation (%)	98.15	97.62	98.23	98.41	98.87	99.16

3.3 Model for power evaluation with road inputs

In this section the evaluation of the power dissipated at the damper level is carried out. To do this, the road profiles have to be generated. In the following sections, a description of how the road profiles are created following the ISO standards is provided and also some experimentally evaluated road profiles are considered. Then, the profiles will be given as inputs to the vehicle S-function and a model for the power evaluation is generated.

3.3.1 ISO road profiles generation

The ISO road profiles have been generated following the procedure explained in Section 1.6.2. The profile is generated from a white noise using a low-pass filter with increasing power spectral density with respect to the frequency. The cut-off frequency of the filter takes into account wavelengths up to $100\,m$. The filter has the form described in Section 2.6.2

$$G(s) = \frac{2\pi\sqrt{G_r V}}{s + \omega_0} \tag{3.3.1}$$

where G_r is the road roughness coefficient, V the vehicle speed and ω_0 is the cut-off frequency. The cut-off frequency is computed as:

$$\omega_0 = \frac{2\pi V}{100} \tag{3.3.2}$$

The roughness coefficients G_r used for the road profile generation are reported in Table 3.4. The model has been used in the Simulink® environment and is shown in Figure 3.6. Several road profiles were generated considering road classes from A to E and different riding velocities ranging from 10 to $130\,km/h$. In this way, the effect of both vehicle velocity and road roughness is considered when filtering the white noise signal.

Table 3.4: *Road roughness coefficient for use in the first-order filter*

Road type	Roughness coefficient G_r
ISO A	1.6E-7
ISO B	6.4E-7
ISO C	25.6E-7
ISO D	102.4E-7
ISO E	409.6E-7

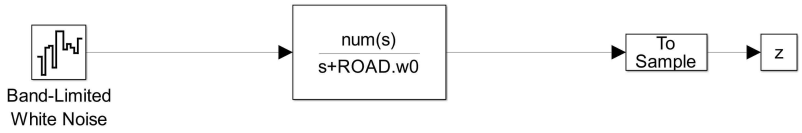

Figure 3.6: *Road profile creator model*

3.3.2 Evaluated road profiles

The simulations were conducted considering two road profiles that have been evaluated on track from the wheel hub acceleration. These two profiles represent one very smooth road and a rough one. Figure 3.7 shows the two roads' altitude variation for both left and right wheel as a function of the driven distance over the first 400 meters. From the analysis of the PSD of the two road profiles it can be noticed that the *smooth* road represents an input that can be considered smoother than the one that could be found in real world highways, because it has been estimated on a test track. On the contrary, the *rough* profile is worse than the typical urban road, and for this reason it is also more energetic. When comparing the positioning of these road profiles to the ISO standard, it can be seen that the *smooth* profile is less energetic than the ISO A standard profile, while the *rough* profile is comparable to an ISO C. In Figure 3.8, the frequency content of the ISO profiles, as well as the evaluated road profiles, is compared in a frequency range of $0 - -20\,Hz$.

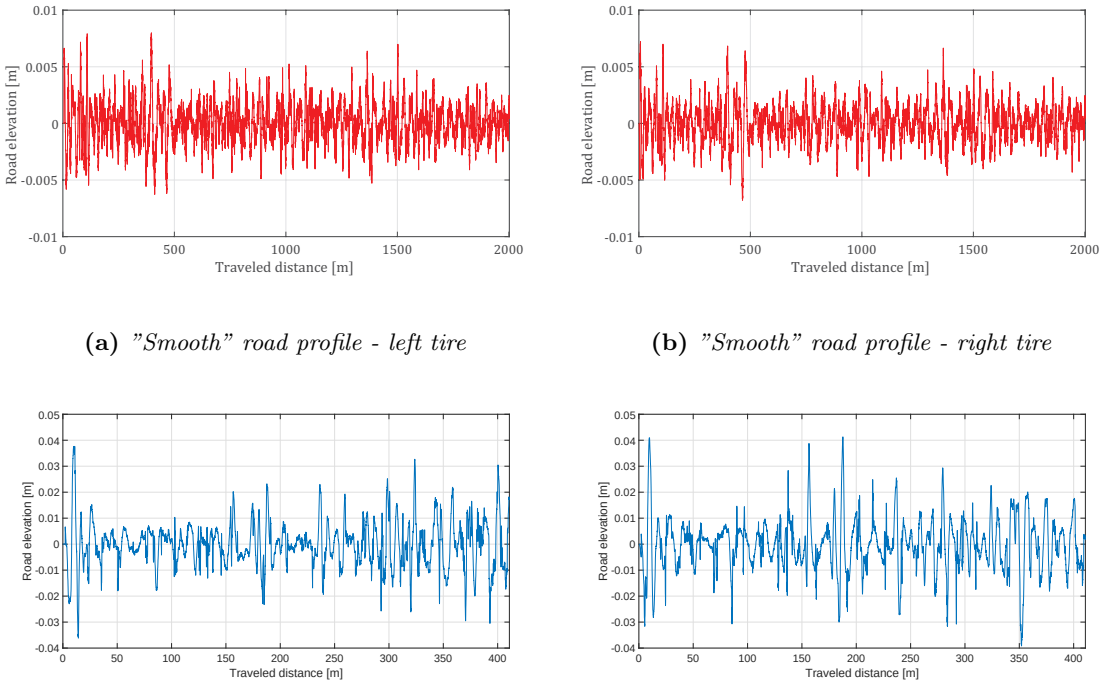

(a) *"Smooth" road profile - left tire*

(b) *"Smooth" road profile - right tire*

(c) *"Rough" road profile - left tire*

(d) *"Rough" road profile - right tire*

Figure 3.7: *Evaluated road profiles*

3.3.3 Model creation

In this section the model for the evaluation of the dissipated power at a damper level is addressed. The model analyzed in the previous section must now be modified in order to:

- accept as input the road roughness profiles for each tire
- give as output the instantaneous dissipated power
- compute the average power dissipated during the whole simulation

The riding simulations for the power evaluation are carried out on a straight road. The inputs are provided to the S-function through the *Road inputs* block (Figure 3.9) as time series, i.e. each value of the road altitude is associated with a particular time instant that will reflect the processing time of the simulation. In the case of ISO profile generator, the output of the filter provides values associated with a time instant, because of the presence of the vehicle velocity as its own parameter. In the case of the estimated road profiles, the

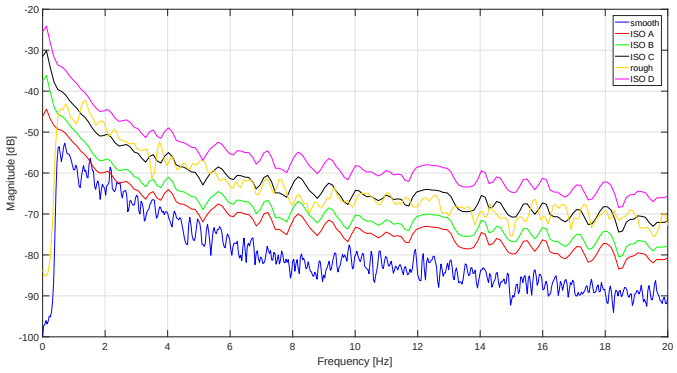

Figure 3.8: *Frequency content of road profiles*

road altitude is given as a function of the distance traveled, so for each simulation the time series must be adapted accordingly to the vehicle running speed. The passive damper model is now included in the subsystem named *Damper system* that includes the look-up tables previously discussed in this thesis. The instantaneous power is computed inside the block *Dissipated power* receiving as input both the dampers' velocities and forces and giving as outputs the instantaneous power for each corner, which is then used to compute the average value, in the following block named *Average*. The instantaneous power is also sent to the workspace for further analyses. The results obtained with this model will be discussed in the next chapter of this thesis. The next step is the implementation of the regenerative damper inside the model, thus eliminating the passive damper. However, before the analysis of the complete model, a deep insight is given to the model of the regenerative damper, that is an EHA (Electro Hydraulic Actuator), and all its components.

3.4 Regenerative damper model

As anticipated, the regenerative damper model that will be used in this thesis will be an Active damper with Electro-Hydraulic Actuator (EHA). The model of this damper has been provided by Magneti Marelli. The EHA is an electrically powered actuator incorporating a controlled direction electric motor and hydraulic pump. The regenerative damper model is made up of three main subsystems: the three-tube hydraulic cylinder, the Electro-Hydraulic Actuator and the External orifice.

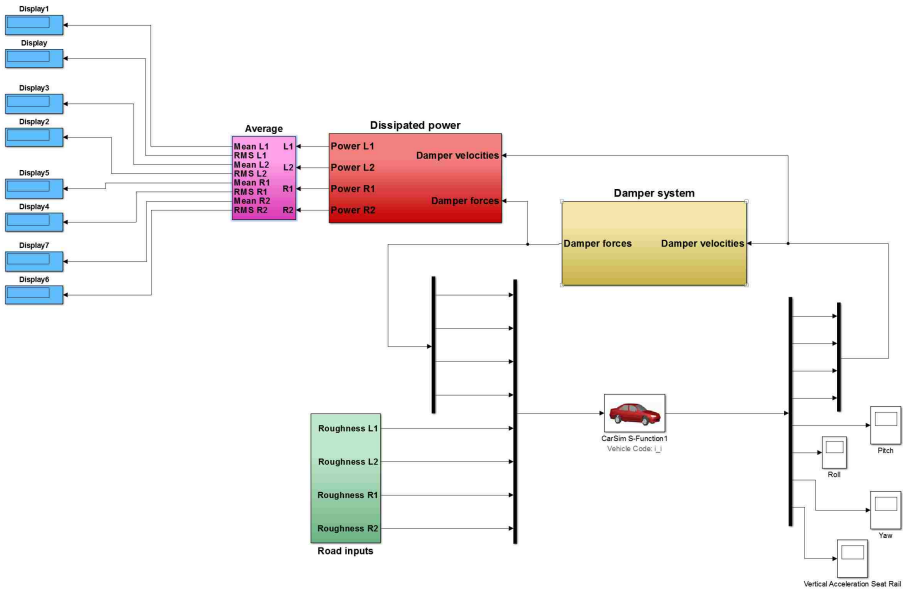

Figure 3.9: *Model for dissipated power computation caused by road irregularities*

Three-tube hydraulic cylinder It is composed by three chambers, that will be named with letters from A to C. The Chamber A is the one where the piston and rod is present. A tube connects this chamber with the hydraulic pump, rigidly connected to the electric generator. The Chamber B is the one in-between Chamber A and C and it is connected to them through check valves. The Chamber C is the most external one and is the one where the other extremity of the tube connected to the hydraulic pump is present, so the damper oil is recirculated between Chamber A and B. A schematic diagram of the damper is shown in Figure 3.10.

Electro-Hydraulic Actuator The EHA model includes the Permanent Magnet Synchronous Machine and Motor and Pump characteristic model. With this block, the amount of recirculated oil flow, the current, and the angular velocity of the generator are obtained from the initial pressure differential as input.

External Orifice It is a hydraulic orifice model with flow rate as input and a pressure variation as output.

All the components of the regenerative model will be described in more detail in the following sections.

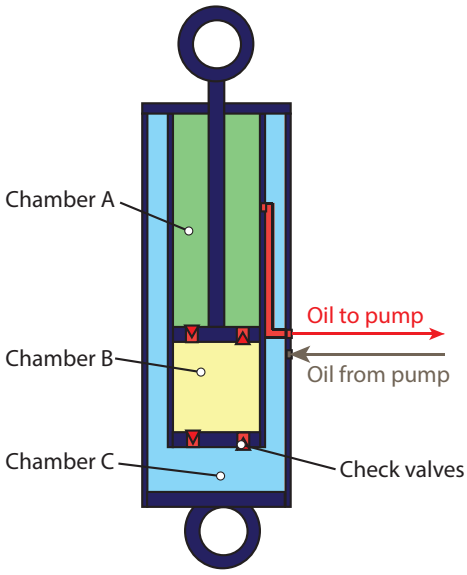

Figure 3.10: *Schematic of the shock absorber - Insight of the chamber configuration*

3.4.1 Hydraulic cylinder

The hydraulic cylinder is the component receiving as input the velocity coming from the vehicle S-function. As already mentioned in the brief introduction, the hydraulic cylinder is made-up of three chambers. The pressure in the three chambers is computed to both evaluate the damper force and the pressure differential between the chambers A and C, that is equal to the one of the EHA. Equation 3.4.1 shows how the pressure in chamber A is computed.

$$(Q_g + v_{in}A_r - Q_{top})k_h = \frac{dP_1}{dt} \tag{3.4.1}$$

where Q_g is the volumetric flow passing through the hydraulic pump, v_{in} the velocity input coming from the vehicle S-function, A_r the area of the piston considering the rod, Q_{top} the volumetric flow passing through the valve between Chamber A and B, k_h is a pressure drop coefficient and P_1 the pressure in Chamber A. Similarly the pressure P_2 in Chamber B is evaluated according to equation 3.4.2.

$$(Q_{top} - v_{in}A_{nr} - Q_{bot})\,k_h = \frac{dP_2}{dt} \tag{3.4.2}$$

where A_{nr} is the complete piston area without considering the rod, Q_{bot} the volumetric flow between Chamber B and C. In a similar way the pressure in Chamber C has been

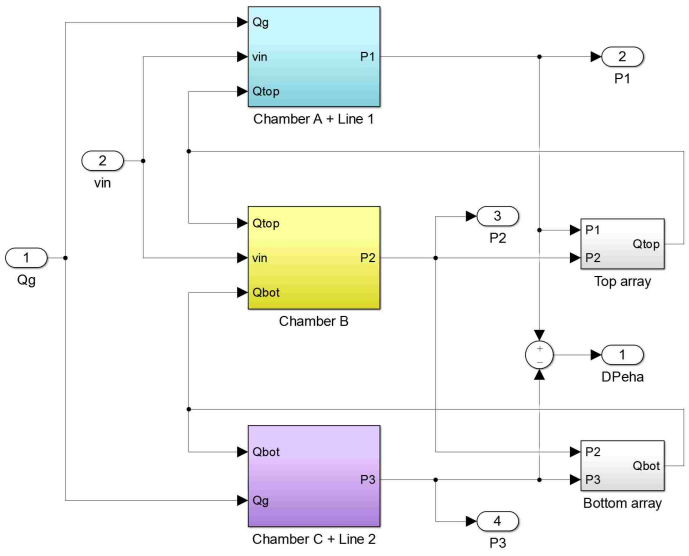

Figure 3.11: *Model of the hydraulic cylinder*

computed also considering the presence of the accumulator. In Figure 3.11 the full model of the hydraulic cylinder is shown.

3.4.2 Electro hydraulic actuator

The EHA model contains a Permanent Magnet Synchronous Motor model receiving inputs from the motor and pump mechanics model. Considering the motor and pump characteristic model, it receives as input the pressure difference ΔP_g and the torque value T_m from the PMSM model. When considering the PMSM model, the input is the angular velocity coming from the pump characteristic, that is considered rigidly connected to the motor shaft. Inside the block, the direct-axis and quadrature currents are computed according to equations 3.4.3 and 3.4.4 respectively.

$$V_q - \omega_m k_m - \omega_m L p i_d - i_q(R + R_{ext}) = L\frac{di_q}{dt} \tag{3.4.3}$$

$$V_d + \omega_m L p i_q - i_d(R + R_{ext}) = L\frac{di_d}{dt} \tag{3.4.4}$$

where V_q and V_d the quadrature and direct-axis voltage respectively, ω_m the angular velocity, k_m the motor constant, L the inductance, p the number of paired poles, i_q and i_d the quadrature and direct-axis current respectively and R and R_{ext} the internal and external

resistance. The output torque is thus calculated considering from the quadrature current as in equation 3.4.5

$$T_m = \frac{3}{2} k_m i_q \tag{3.4.5}$$

The complete model of the EHA is shown in Figure 3.12.

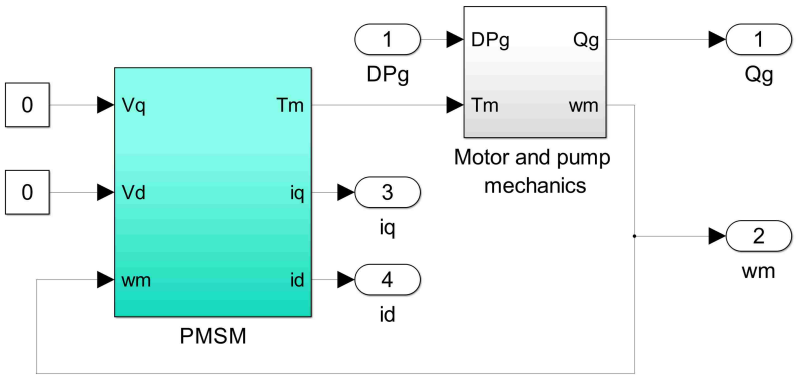

Figure 3.12: *EHA model*

3.4.3 Complete damper model

According to the descriptions of the different components, in this section the complete scheme of the damper is analyzed. In this model it is possible to notice that

- the differential pressure coming from the hydraulic cylinder is sent as output to the EHA after having summed up also the pressure differential coming from the external orifice

$$\Delta P_g = \Delta P_{EHA} + \Delta P_{or}$$

- the hydraulic cylinder receives as input the volumetric flow rate Q_g of the oil passing through the pump and the velocity measured at the damper extremities

- the damper force is computed from the pressure outputs P_1 and P_2 according to the following equation

$$P_1 A_r - P_2 A_{nr} = F_{damp}$$

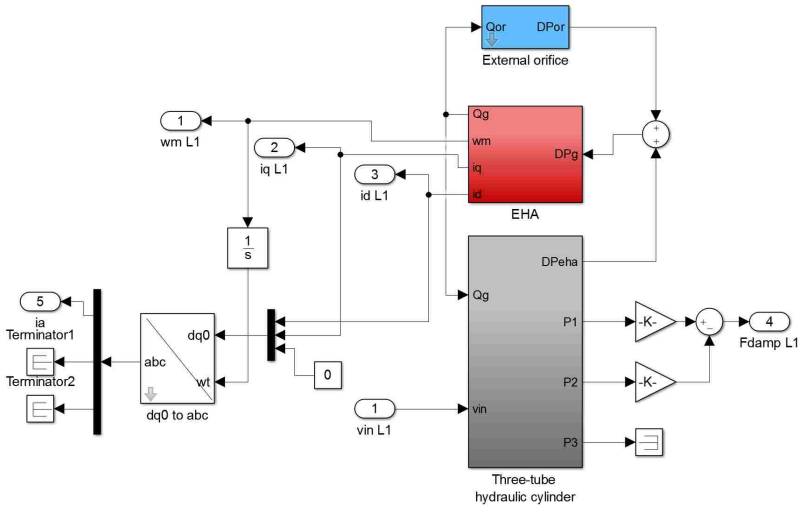

Figure 3.13: *Complete damper model*

3.5 Vehicle model with regenerative dampers

In this section the regenerative damper model is put inside the complete vehicle model. Each of the look-up tables that were used during the first steps of the model preparation are now replaced by the regenerative dampers. Nothing is dramatically changed inside the model. There is now a block including the characteristics of the new dampers, but the inputs and outputs received are the same, i.e. the damper compression rates and forces respectively (Figure 3.14). Each input is internally sent to its damper and the output force is sent back to the vehicle S-function. Since the output currents of the generator are available as outputs from the dampers, it is possible to evaluate the energy recovery efficiency of the damper η_{damp}. The output power available is than compared to the power dissipated by the damper and the efficiency is computed. However, in order to have a complete scheme of the damper efficiency, it is necessary to repeat all the simulations considering all the speeds associated with all the specified road profiles. The ratio of these two quantity is directly computed inside the *regenerative damper* block according to the scheme shown in Figure 3.15. The electrical and damper power is evaluated from each of the damper and then summed up. The efficiency is then computed considering the ratio between the root mean square values. The results obtained will be shown in the following chapter.

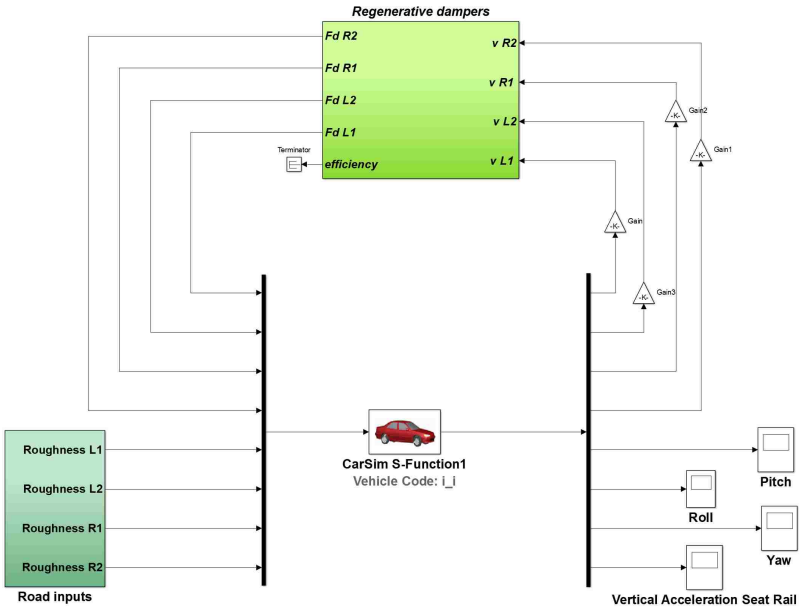

Figure 3.14: *Vehicle model with regenerative dampers*

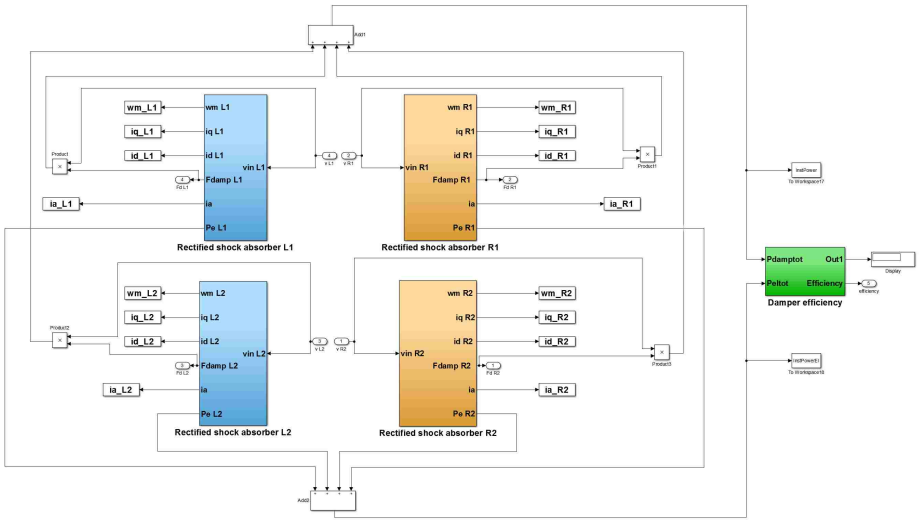

Figure 3.15: *Damper scheme - efficiency evaluation*

Chapter 4

Simulation results and discussion

In this chapter, all the results from the outputs of the different simulated models are reported. At first the results concerning the dissipated energy by a conventional damper and the effect of the vehicle velocity and road profile on the amount of energy that is wasted are shown. Then the same procedure is followed to analyze the behavior of the regenerative dampers. At first an energetic analysis is presented, taking into account both the dissipated and recovered energy, in order to evaluate the regenerative damper system efficiency, because non-idealities are included in the regenerative damper model. Then, the results after the damper optimization are also shown in order to evaluate the real effectiveness of the whole system.

4.1 Simulations with conventional dampers

As already announced in the introduction, as a first step, the amount of energy that is dissipated by the damper in different road conditions and vehicle velocities is simulated using the model shown in the previous chapter in Figure 3.9. At first the average values of dissipated power considering ISO road profiles are reported in Table 4.1.

The road profiles are generated according to the procedure described in Chapter 3. For each road class, several simulations have been run with different velocities. In particular,

Table 4.1: *Average power values at vehicle level with passive dampers - Units are [W]*

	A	*B*	*C*	*D*	*E*
$10\,km/h$	5.82	17.21	63.70	253.12	1012.4
$20\,km/h$	9.55	32.49	125.88	506	1907.8
$30\,km/h$	13.32	47.84	188.16	751.8	2723.2
$40\,km/h$	17.09	63.24	250.46	992.8	3388.2
$50\,km/h$	20.89	78.64	312.6	1216	3986.8
$60\,km/h$	24.70	94.02	374.6	1432.8	4548
$70\,km/h$	28.60	109.56	436.4	1646.4	–
$80\,km/h$	32.52	124.95	497.9	1863.2	–
$90\,km/h$	36.44	140.51	559.3	2072.9	–
$100\,km/h$	40.07	155.35	618.6	2272.7	–
$110\,km/h$	44.1	170.93	678.8	2464	–
$120\,km/h$	47.95	186.26	738.4	–	–
$130\,km/h$	51.71	201.42	796.8	–	–

the velocity values range from 10 to $130\,km/h$ with steps of $10\,km/h$. As it is shown in the table, the energy values are not reported for each velocity and road profiles. Some of them are missing because they don't have a practical meaning because of the physical impossibility of driving at that speed on the specific road, e.g. $130\,km/h$ on road classified as ISO E. The simulations have also been completed with measured road profiles named as *smooth* and *rough* in Chapter 3. The results from these simulations are summarized in Table 4.2. In this case the velocity range used during the simulations is $10 - -60\,km/h$ for the *rough* profile, and $70 - -130\,km/h$ for the *smooth* one. These results, both the ones from ISO and measured profiles, are then plotted all together considering the effect of the road and of the vehicle velocity separately. The *smooth* profile is expecting to behave better than an ISO A road, while the *rough* profile is in-between the ISO B and ISO C road, so it is a a bit worse than the usual roads that can be found in a urban environment. Now the energy that is recovered during the simulation time is evaluated. The amount of energy recovered is plotted versus the simulation time considering:

Table 4.2: *Average power with measured road profiles - Units in [W]*

Rough		Smooth	
$10\,km/h$	24.27	$70\,km/h$	14.97
$20\,km/h$	79.35	$80\,km/h$	15.31
$30\,km/h$	169.15	$90\,km/h$	16.70
$40\,km/h$	238.58	$100\,km/h$	18.09
$50\,km/h$	314.56	$110\,km/h$	19.60
$60\,km/h$	389.94	$120\,km/h$	21.17
–	–	$130\,km/h$	22.89

1. Constant road profile and variable vehicle speed

2. Constant vehicle speed and different road profile

In Figure 4.1 the results for the average dissipated power are plotted against the vehicle speed with the different road profiles, both ISO and measured. The results in Table 4.1 show

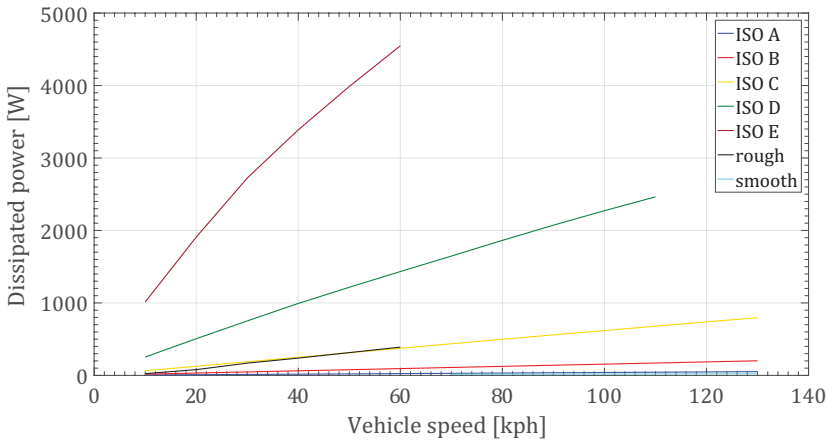

Figure 4.1: *Power dissipated as function of vehicle speed for different road profiles with passive dampers*

the average power that can ideally be recovered by the damper. As expected, the values

increase with rougher profiles and higher speeds. From this table it is possible to highlight that on a highway with speeds from 100 kph to 130 kph, an ideal value of $40 - -50\,W$ can be harvested. However, the most promising scenario is the urban one that can be associated with an ISO C road profiles with vehicle speeds ranging from 30 kph to 60 kph where an amount of harvested power from 190 up to 370 W could be expected. The same results were also evaluated for the identified road profiles. In this case the power dissipated is in the range $18 - -20\,W$ in the case of *smooth* profile, and $170 - -390\,W$ for the *rough* one. As expected, the values are lower for the *smooth* profile when compared to the ISO A because it was expected to be less energetic. The values from the *rough* profile are instead comparable with the ones obtained by ISO C. The amount of dissipated energy increases almost linearly with vehicle speed (Figure 4.1). In the same figure we can also notice that the slope of the curve increases when using a more energetic road profiles, meaning that in this case the amount of power increase could be higher even if considering a smaller velocity variation.

4.1.1 Comfort analysis

In order to have some comfort parameters to be compared from both model, the vertical, pitch and roll accelerations are evaluated in terms of RMS values. These values are calculated for both highway and urban driving conditions, in particular:

- *Highway*: ISO A road profile with vehicle speed of 110 and 130 kph
- *Urban*: ISO B and ISO C road profile with vehicle speed of 50 kph

The results obtained during the simulation on ISO C road profile are shown in Figure 4.3. The RMS values of all accelerations are now evaluated for each driving condition and the values are reported in Table 4.3. The values in this Table will be compared to the ones obtained with the regenerative damper in Section 4.3.

4.2 Simulations with regenerative dampers

When considering the full-vehicle model with regenerative dampers, as described in Chapter 3, many more variables must be considered when evaluating the performance of the damper.

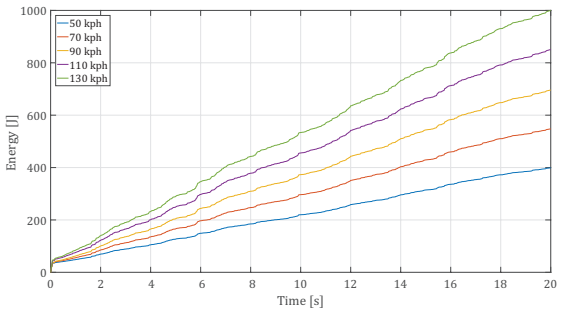

(a) *Road ISO A*

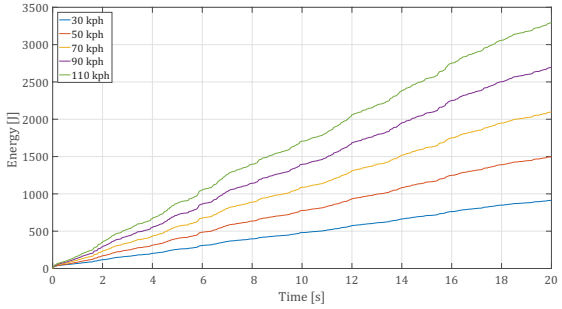

(b) *Road ISO B*

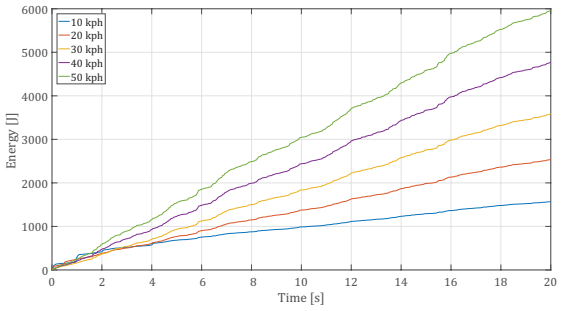

(c) *Road ISO C*

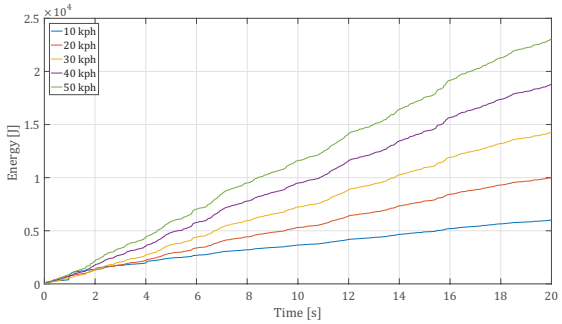

(d) *Road ISO D*

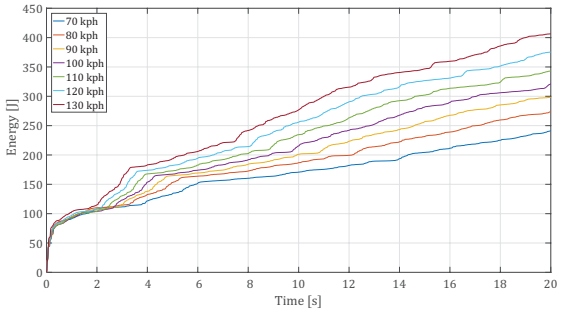

(e) *Road 'smooth'*

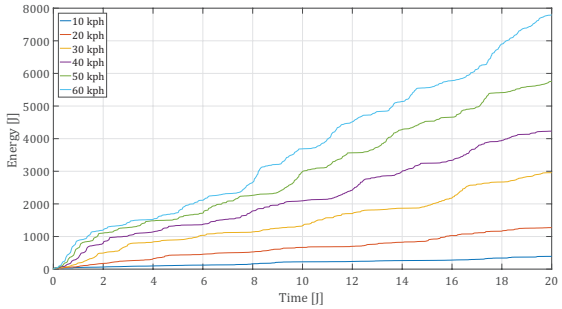

(f) *Road 'rough'*

Figure 4.2: *Harvestable energy with passive dampers during the simulation time*

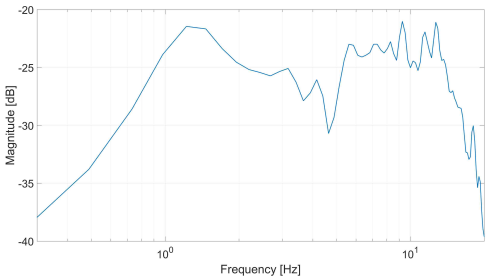

(a) *Pitch Acceleration power spectrum of vehicle sprung mass*

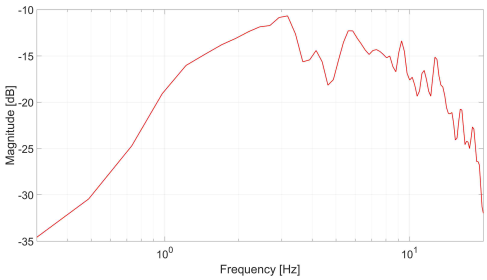

(b) *Roll Acceleration of vehicle sprung mass*

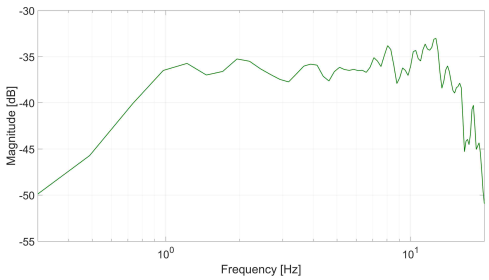

(c) *Vertical Acceleration of vehicle sprung mass*

Figure 4.3: *Sprung mass accelerations for vehicle comfort evaluation - ISO C road profile - Vehicle speed* 50 *kph*

Together with road conditions and vehicle speed, the shunt resistance applied to the generator circuit is considered. This resistance is a control parameter, because, by acting on it, it is possible to change the response of the damper, making it stiffer or softer. Another factor that should be considered is the fact that the damper does not convert mechanical energy into electrical energy with constant efficiency. For this reason, a sensitivity analysis on how the damper characteristics vary as a function of the shunt resistance is necessary.

4.2.1 Damping coefficient and dissipated power analysis

In order to evaluate how the shunt resistance affects the damper, several simulations have been done using three variables: vehicle speed, road profile and shunt resistance. In the post-processing phase, the damping coefficient variation and the dissipated power are plotted against the shunt resistance. Some of these plots are shown in Figure 4.4. From Figure

Table 4.3: *Sprung mass RMS acceleration values - Passive damper model*

	a_{z_RMS} $[m/s^2]$	a_{p_RMS} $[rad/s^2]$	a_{r_RMS} $[rad/s^2]$
ISO C - 50 kph	0.801	0.321	0.863
ISO B - 50 kph	0.470	0.188	0.462
ISO A - 130 kph	0.402	0.156	0.381
ISO A - 110 kph	0.377	0.148	0.353

4.4, it can be noticed that the amount of power to be dissipated is almost constant throughout the shunt resistance range. On the contrary, the damping coefficient varies so that it remains almost constant in the shunt resistance range of $1 - -10\,m\Omega$. The damping coefficient decreases down to values of about $1000\,Ns/m$ with a shunt resistance of about $1\,\Omega$. Further increases in external resistance are not effective in terms of damping coefficient variation. All the damping values are computed as linear approximation of the force-velocity points recorded during the simulation time. Moreover it is interesting to understand how the damping coefficient interval of variability changes with the different input frequencies, because, as is shown in Figure 4.4, the damping coefficient in the range $1 - -70\,m\Omega$ varies with the considered frequency input. To analyze this phenomenon, the damping coefficient is plotted against the shunt resistance at different road inputs and vehicle speeds (Figure 4.5). It can be noticed that with very low shunt resistances the gap can be as high as 2000 Ns/m on the same road with different vehicle speed. However, this situation occurs only in case of very over-damped systems and is not common during everyday vehicle usage. If considering the range above $60 - 70\,m\Omega$, the difference is greatly reduced and is in part due to the linear approximation of the damping coefficient.

4.2.2 Harvested power from the regenerative shock absorbers

In the full vehicle model with the regenerative shock absorbers model, the harvested power can be computed at vehicle level. This electrical power is evaluated from the direct-axis and quadrature current, according to equation 4.2.1.

$$P_h = \frac{3}{2} R_{ext}(i_q^2 + i_d^2) \tag{4.2.1}$$

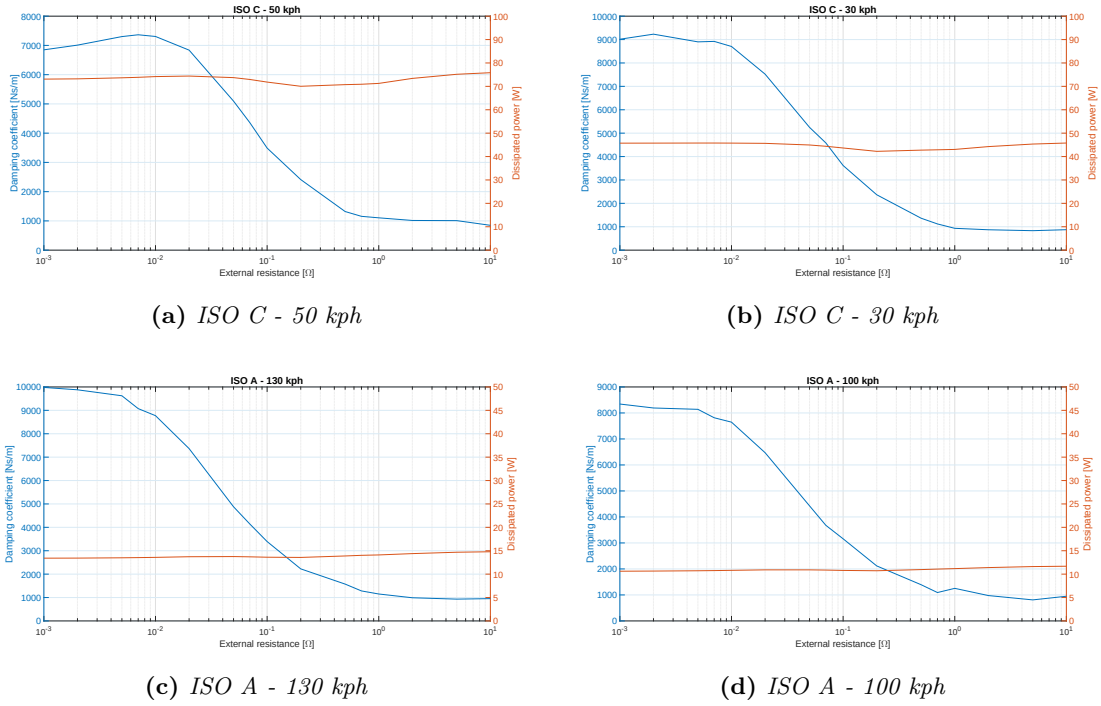

(a) *ISO C - 50 kph*

(b) *ISO C - 30 kph*

(c) *ISO A - 130 kph*

(d) *ISO A - 100 kph*

Figure 4.4: *Damping coefficient and dissipated power variation - left front vehicle corner*

The average value is then computed from the instantaneous harvested power P_h and this value is considered for future considerations. This procedure has been followed for each road profile, each vehicle velocity and external resistance. The values obtained are plotted in a 3D map in Figure 4.6. The maps show the harvested power at vehicle level on a specific road profiles with different shunt resistance - vehicle velocity configuration. It can be noticed that the curves at constant velocity have a kind of parabolic shape and that highest amount of harvested power is obtained for a shunt resistance value of about $140\,m\Omega$. In this case, values up to $178\,W$ can be harvested by the suspension system in case of ISO C profiles. In case of less energetic road profiles, the amount of harvestable power is greatly decreased down to $34\,W$ at vehicle level. The efficiency of the damper is also evaluated at this point since both the harvested and the dissipated power are known. In Figure 4.7 the efficiency map of the damper is shown. The efficiency is constant along the velocity range, so it depends only on the shunt resistance. The maximum value is achieved for about the same resistance value of the harvested power peak, because of the fact that, as previously

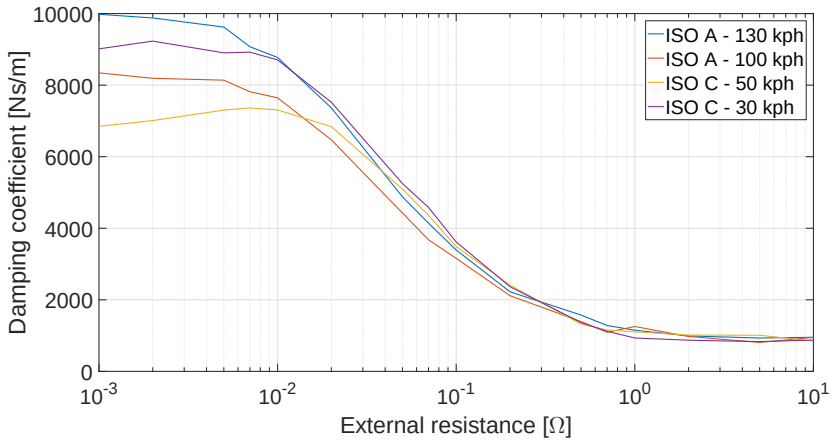

Figure 4.5: *Damping coefficient variation as function of external resistance*

presented in Figure 4.4, the dissipated power almost remains constant along all the shunt resistance range. Values up to 62% can be achieved with an appropriate shunt resistance choice.

4.2.3 Comfort evaluation

In order to evaluate the benefits on the driving comfort, the vehicle sprung mass accelerations (vertical, pitch and roll) are evaluated. In this case the outputs are directly taken from CarSim®and filtered with the ISO 2631 filter. The output is filtered in order to have a response that is more similar to that of the human body, which is more sensitive to some frequencies in the range of $4 - -8\,Hz$. The same procedure for harvested power evaluation was also used for vertical, pitch and roll accelerations. Several 3D maps have been used also in this case to understand the behavior of the suspension in different road conditions, vehicle speeds and shunt resistances. The results are shown in Figure 4.8. The surface shape in this case is very different to the one of the harvested power. The root-mean-square value of the sprung mass vertical acceleration increases with higher velocities and low shunt resistance values. It can also be noticed that the curves at constant velocity tend to an asymptotic behavior for shunt resistance values higher than $90\,m\Omega$ in case of the ISO A profile, and higher than $200\,m\Omega$ for the ISO C road profile. With the same procedure the roll and pitch accelerations have been plotted on a 3D map and the results are shown re-

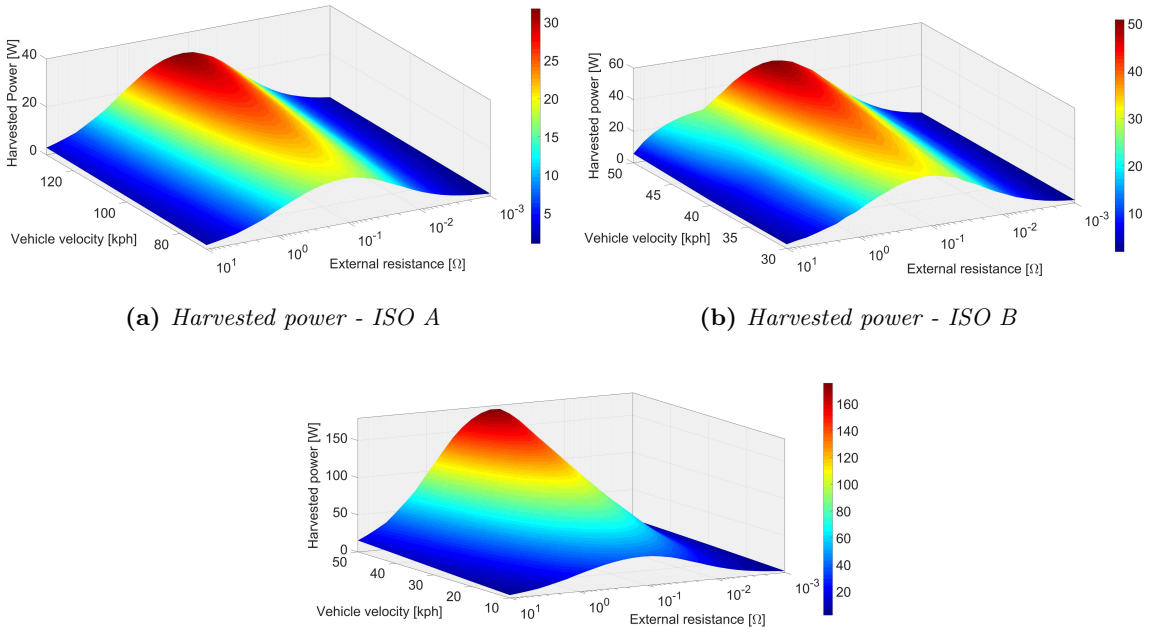

(a) *Harvested power - ISO A*

(b) *Harvested power - ISO B*

(c) *Harvested power - ISO C*

Figure 4.6: *Harvested power in different road conditions*

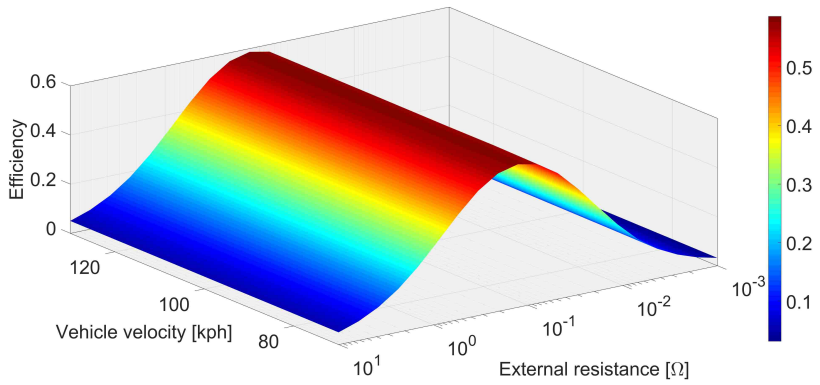

Figure 4.7: *Efficiency map - Values evaluated on ISO A road with vehicle speed ranging from* 70 *to* 130 *kph*

spectively in Figure 4.9 and 4.10. The roll acceleration surface shows a valley in the range of $70 - -200\,m\Omega$. In case of higher or lower shunt resistance values the roll acceleration increases again. This range almost remain constant for the different road profiles, but it is a bit shortened to $80 - -160\,m\Omega$ for higher vehicle velocities on the same road profile.

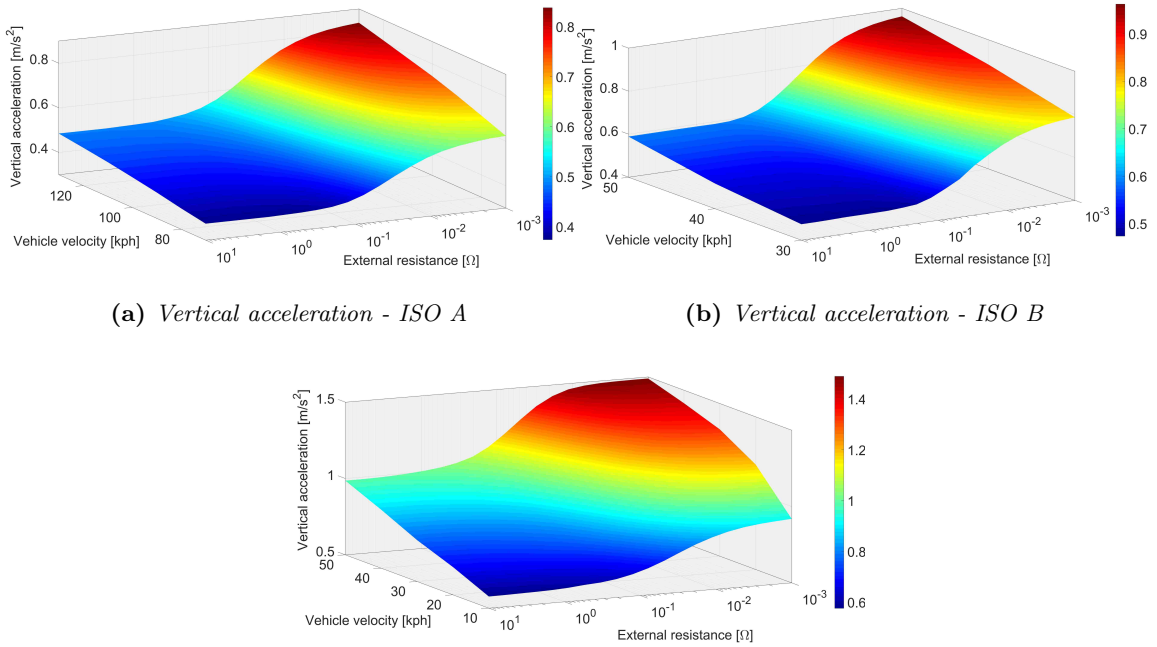

(a) *Vertical acceleration - ISO A*

(b) *Vertical acceleration - ISO B*

(c) *Vertical acceleration - ISO C*

Figure 4.8: *Vertical acceleration in different road conditions*

The pitch acceleration surface has a similar behavior of the roll one. Moreover, the shunt resistance interval is $80 - -190\,m\Omega$ for ISO A profile, and $110 - -210\,m\Omega$ for more the ISO C. Regarding the comfort evaluation, it is evident that the shunt resistance value giving the highest amount of recoverable energy is also compatible with the interval giving the lowest sprung mass acceleration, thus improving the general driving comfort.

4.2.4 Road handling

Another very important parameter to consider for the vehicle behavior is the road handling index (RHI). It is important to evaluate if the wheel may not experience enough contact force with the ground or even lose contact. This phenomena are unsafe for the driver and could potentially lead to lose control of the vehicle. It depends on the dynamic and static force between tire and ground. The wheel will lose ground contact with the ground when the ratio is greater than or equal to one. It is defined as

$$RHI = \frac{k_u(z_u - z_w)}{g(m_u + m_s)} \tag{4.2.2}$$

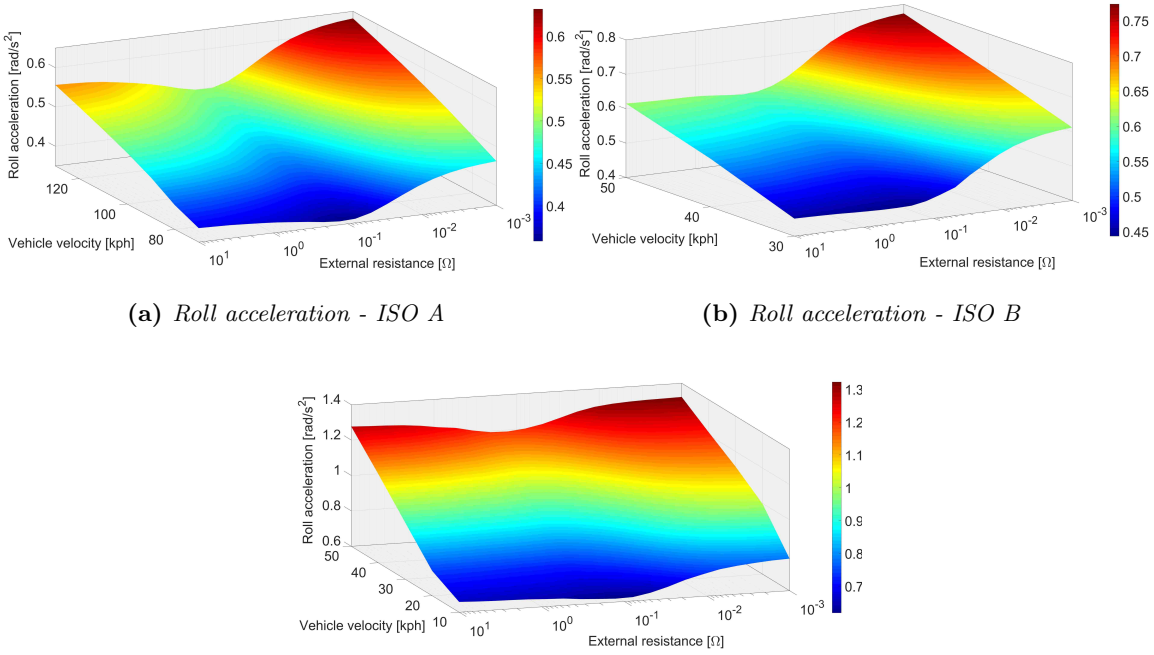

(a) *Roll acceleration - ISO A*

(b) *Roll acceleration - ISO B*

(c) *Roll acceleration - ISO C*

Figure 4.9: *Roll acceleration in different road conditions*

where k_u is the spring stiffness, z_u the vertical displacement of the unsprung mass, z_w the vertical displacement of the wheel, g is the gravity acceleration, m_u the unsprung mass and m_s the sprung mass of the considered corner. The results obtained for the RHI are reported as RMS values. The results are depicted in Figure 4.11. The behavior of the RHI is not so far from that of the roll acceleration. The surface valleys are in the same range of $90 - -160\,m\Omega$. This is a very important result because of the fact that at the same time it is possible to obtain a good amount of harvested power without having a negative effect on comfort or road handling capabilities.

4.2.5 Considerations on shunt resistance choice

From all the previous findings the main outcomes are:

- the harvested power has a parabolic shape with its vertex in the $100 - -150\,m\Omega$ range. In that range, the efficiency is also maximum because the dissipated power is almost constant along all the resistance range

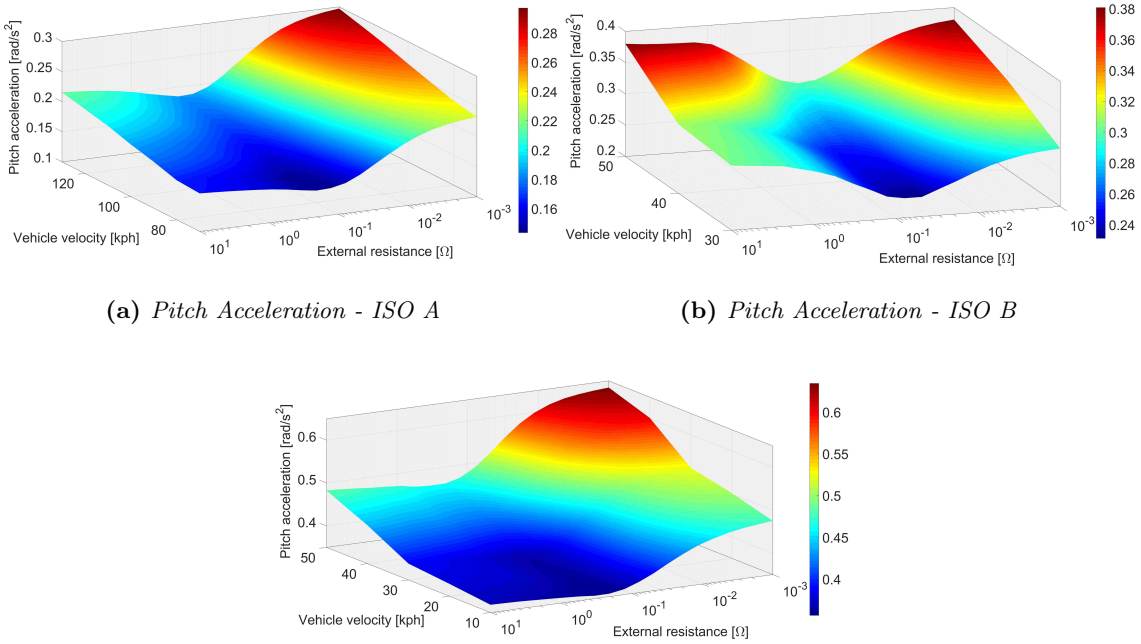

(a) *Pitch Acceleration - ISO A*

(b) *Pitch Acceleration - ISO B*

(c) *Pitch Acceleration - ISO C*

Figure 4.10: *Pitch acceleration in different road conditions*

- the comfort analysis shows that the sprung mass accelerations (vertical, pitch and roll) are minimized or very close to their minimum value ($< 5\%$ of difference) in the above mentioned range

- the handling performance of the vehicle is not compromised because of the fact that the RHI is minimum in the same range. This is due to the fact that the damper is designed in order to behave near the optimal damping coefficient, allowing a very good compromise between sprung mass accelerations reduction and road holding capabilities

After all these considerations, a shunt resistance of 140 $m\Omega$ has been chosen in order to have a complete optimization of the comfort and road handling capabilities, having in mind that the damper is also working at its maximum efficiency point. With this configuration, the following outputs will be evaluated in the next section:

- reduction in sprung mass accelerations (vertical, pitch and roll) with respect to the

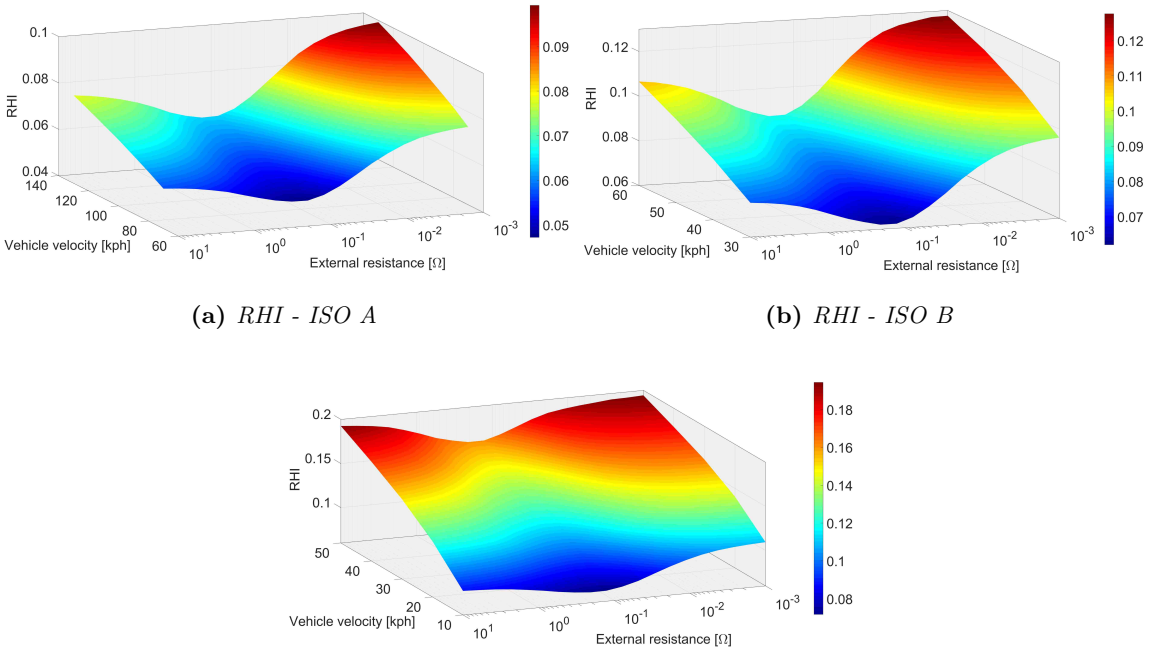

(a) *RHI - ISO A*

(b) *RHI - ISO B*

(c) *RHI - ISO C*

Figure 4.11: *RHI in different road conditions*

passive model

- evaluation of the CO_2 reduction considering that the harvested power need is not provided by the alternator and the driving conditions are chosen according to the U.S. Department of Transportation vehicle usage statistics
- according to the above mentioned usage statistics, the following road profiles will be used for each road condition:
  - *Highway condition*: ISO A road profile with 110 *kph* and 130 *kph* vehicle speeds
  - *Urban condition*: both ISO B and ISO C because with vehicle speed of 50 *kph* because of the high variability of road that can be found in different urban environments

4.3 Dynamic improvements

As already stated in the previous sections, the external resistance value has been chosen in order to have a minimization of the sprung mass accelerations. For this reason, the regenerative vehicle model is now compared to the passive one to quantify the achieved improvements. The mission profile described in Section 4.2.5 has been followed for both the passive and regenerative models. The results are shown in Table 4.4. As we can notice

Table 4.4: *Sprung mass RMS acceleration values and harvested power - Regenerative damper model*

	a_{z_RMS} $[m/s^2]$	a_{p_RMS} $[rad/s^2]$	a_{r_RMS} $[rad/s^2]$	$P_h[W]$
ISO C - 50 kph	0.767	0.311	0.847	134.3
ISO B - 50 kph	0.456	0.182	0.454	65.78
ISO A - 130 kph	0.381	0.146	0.370	46.41
ISO A - 110 kph	0.355	0.137	0.341	39.91

from this table the RMS values of the vehicle accelerations are always lower than the ones obtained with the passive dampers in Table 4.3. However, to have a better idea of what is the improvement, in Table 4.5 the percentage difference between the two tables was evaluated. So it can be noticed that an improvement in the sprung mass accelerations is

Table 4.5: *Percentage difference of sprung mass RMS acceleration values between passive and active model*

	a_{z_RMS} [%]	a_{p_RMS} [%]	a_{r_RMS} [%]
ISO C - 50 kph	-4.3%	-2.8%	-1.8%
ISO B - 50 kph	-2.9%	-3%	-1.6%
ISO A - 130 kph	-5.7%	-7.1%	-3.3%
ISO A - 110 kph	-5.1%	-5.9%	-2.6%

obtained ranging from about 2 to 7%. A greater improvement could potentially be obtained but, in that case, the amount of harvested energy would have been more than ten times less.

4.4 Energy harvesting capabilities

In this section, the harvestable energy according to the vehicle usage statistics from the U.S. Department of Transportation is computed. According to these statistics, the average mileage is $13,476\,\text{mi/year}$, i.e. $21687\,\text{km/year}$. Of this distance about the 55% is traveled on highway and 45% on urban roads. According to these data:

- about $12,000\,km$ will be traveled on a highway and the harvested power in this case, considering a vehicle speed of $110\,kph$ is about $40\,W$
- the remaining distance is traveled on urban roads, and the harvestable power ranges from 65 to $134.3\,W$ if a road profile ISO B or ISO C is considered

For the urban profile both ISO B and ISO C profiles are taken into account because of the high variability that can be encountered in different urban environments, and because of the lack of a regulation indicating the most adequate road profile for this driving condition. From these considerations it comes out that:

- on a highway the energy harvested during the whole year is $15.4--15.7\,MJ$ depending on the vehicle speed
- on a urban road the harvested energy ranges from $45.9--96.3\,MJ$ depending on the roughness of the road (ISO B or ISO C)

On average the harvested power during the vehicle usage ranges from 60 to $108\,W$ depending on the type of vehicle usage.

4.5 CO_2 savings evaluation

The CO_2 saving has been evaluated according to the guidelines in [40]. The emission reduction is calculated by using the following expression:

$$S_{CO_2} = \frac{\eta_{conv} P_g V_{PE} CF}{\eta_{alt} V} \tag{4.5.1}$$

where V_{PE} describes the reduced fuel consumption with a reduction of required power at a particular point of the engine map and represents the marginal engine's efficiency. Following

the 'Willans approach', the consumption of effective power is nearly constant and almost independent from engine speed at low engine loads. Another important factor to consider

Table 4.6: *Values of consumption of effective power for gasoline and diesel engines*

Type of engine	**Consumption of effective power** $[l/kWh]$
Gasoline	0.264
Diesel	0.22

in equation 4.5.1 is the alternator efficiency η_{alt} essential for the conversion from mechanical into electrical power and vice versa. An efficiency value of 0.67 is considered. CF is the conversion factor from fuel consumption to CO_2 emissions. In Table 4.7 typical values for both gasoline and diesel engines are shown. The other factors influencing the CO_2 emissions

Table 4.7: *Values of conversion factor from fuel consumption to CO_2 emission for gasoline and diesel engines*

Type of engine	**Conversion factor** $[gCO_2/l]$
Gasoline	2330
Diesel	2640

are the power converter efficiency that in this case is 0.9, the harvested power from the four shock absorbers P_g and the vehicle speed V. Following this procedure, the results obtained are shown in Table 4.8. It is possible to notice that in highway conditions the amount of saved CO_2 is about $0.3\,g/km$, while in urban roads the amount of CO_2 saved is between 1.1 and $2.7\,g/km$. Considering that the analyzed vehicle has CO_2 emissions between 100 and $150\,g/km$, the saving that has been obtained is between the 0.2% and 1.8% depending on the driving condition. So, according to the DOT usage statistics the average value of CO_2 saved during the entire use of the vehicle is between 0.8 and $1.5\,g/km$.

Table 4.8: *Values of CO_2 savings per kilometer for both gasoline and diesel engines*

	$\mathbf{S_{CO_2}}$ **Gasoline [g/km]**	$\mathbf{S_{CO_2}}$ **Diesel [g/km]**
ISO A - 110 kph	0.30	0.28
ISO A - 130 kph	0.29	0.27
ISO B - 50 kph	1.09	1.03
ISO C - 50 kph	2.71	2.56
DOT (ISO A + ISO B)	0.7	0.69
DOT (ISO A + ISO C)	1.4	1.35

Chapter 5

Conclusions and recommendations

In this thesis, the model of regenerative hydraulic vehicle suspension, which can generate electric power from road irregularities, was analyzed and integrated into a full vehicle model of a segment C car. The aim of this project is to provide a complete model to predict the harvestable power, the CO_2 emission reduction and also the dynamic performance improvement of this kind of regenerative damper. A full assessment of the performance of this kind of damper is carried out, providing a complete analysis of the chassis motion, harvestable power and road handling characteristics as a function of the external resistance of the damper (the control parameter), the vehicle speed and road profile. The full vehicle model is studied in CarSim®, while the regenerative damper is developed in Matlab®. The existing interface between these two softwares was exploited in order to achieve all the results presented throughout the thesis. The model receives as input random road profiles generated according to the ISO 8608 classification. The simulations provide an estimation of harvested power and, hence, of CO_2 reduction. This estimation is also carried out considering the average vehicle usage of a North American customer. The results show that an average value of 1.5 g/km of CO_2 reduction can be achieved considering a mission profile reflecting the vehicle usage statistics from DOT. This value accounts for $1 - 1.5\%$ of the vehicle CO_2 emissions. This reduction is obtained thanks to an average amount of

harvested power of about 100 W. In this thesis, it was chosen to evaluate the urban condition in both ISO B and ISO C road profiles, because of the lack of a regulation indicating the exact profile associated to it, due to the high variability of the phenomenon. These results are obtained without degrading the vehicle comfort and handling characteristics. This has been possible analyzing the behavior of the damper with different shunt resistances and road conditions and choosing an appropriate value in order to maximize the harvested power, and at the same time minimizing the sprung mass accelerations and RHI. A reduction from 2 to 7% of vehicle sprung mass acceleration is achieved thanks to the design of the damper, that shows the optimal value of damping coefficient in proximity of the maximum of the damper efficiency curve. This condition allows to achieve good harvesting capabilities without compromising comfort or handling characteristics, if an appropriate shunt resistance is chosen. All these values are consistent when considering this kind of damper applied on this specific vehicle.

5.1 Recommendations

In this thesis, the CO_2 savings has been evaluated with efficiency values of the engine and alternator coming from EC regulations. In order to improve the accuracy for the evaluation of the CO_2 reduction, the model of an alternator could be inserted into the full vehicle model. An important step, for further development of the model, is the application of a prototype into a vehicle suspension system in order to:

- evaluate all the parameters shown in this thesis (harvested power, chassis accelerations, RHI)
- analyze the correlation between the computational and experimental results
- improve the model according to the new experimental data

A cost estimation for large scale production of the regenerative damper is necessary in order to evaluate if the benefits achieved are worth the increase in production cost, and thus the broader implementation on production vehicles.

Bibliography

[1] United States Environmental Protecion Agency, *Sources of Greenhouse Gas Emissions*, https://www3.epa.gov/climatechange/ghgemissions/sources.html, as June 2016

[2] International Energy Agency, CO_2 *emissions from fuel combustion*, 2015 edition

[3] CC Tech. 2016. 1997-2013 Shock Absorber Information and Replacement. [ONLINE] Available at: *http://tech.corvettecentral.com/2014/06/1997-2013-shock-absorber-information-replacement.* [Accessed 22 July 2016]

[4] TOKICO. 2016. Tokico - Function and structure. [ONLINE] Available at: *http://www.tokico.biz/tokico_product/function_structure/index.html.* [Accessed 4 August 2016]

[5] Vehi.co. 2016. ISO Double Lane Change Test. [ONLINE] Available at: *http://www.vehico.com/index.php/en/applications/iso-lane-change-test* [Accessed 1 August 2016]

[6] B. Heiring, M. Ersoy, *Chassis Hanbook - Fundamentals, Driving Dynamics, Components, Mechatronics, Perspectives*, ATZ, 1st edition, 2011

[7] S.B.A. Kashem, T. Saravana Kannan, T.A. Choudhury, M.A. Choudhury, Sajib Roy, A.A. Safe, M.Ektesabi, R. Nagarajah, *A Comprehensive Study on Suspension System and Tilting Vehicle*, Aust. J. Basic & Appl. Sci., 9(30): 46-53, 2015

[8] Lei Zuo, Pei-Sheng Zhang, *Energy Harvesting, Ride Comfort, and Road Handling of Regenerative Vehicle Suspensions*, J. of Vibeation and Acoustic, Vol. 135, 2013

[9] Lei Zuo, B. Scully, J. Shestani, Y. Zhou, *Design and Characterization of an Electromagnetic Energy Harvester for Vehicle Suspensions*, Smart Mater. Struct., 19(4), p.045003, 2010

[10] Y. Zhang, F. Yu, K. Huang, *A State of Art Review on Regenerative Vehicle Active Suspension*, Proceedings of the 3rd International Conference on Mechanical Engineering and Mechanics (ICMEM), Beijing, China, October 21-23

[11] L. Segel, X. Lu, *Vehicular Resistance to Motion as Influenced by Road Roughness and Highway Alignment*, Aust. Road Res., 12(4), pp. 211-222, 1982

[12] G. Bomarito, *A study on Energy Harvesting Trough the Use of Electromagnetic Dampers in Motion Control Schemes*, Cornell University, 2010

[13] Y. Zhang, X. Zhang, M. Zhan, K. Guo, F. Zhao, Z. Liu, *Study on a novel hydraulic pumping regenerative suspension for vehicles*, J. of the Franklin Institute, 352, pp.485-499, 2015

[14] C. Li, P.W. Tse, *Fabrication and testing of an energy-harvesting hydraulic damper*, Smart Mater. Struct., 22, p.065024, 2013

[15] Z. Parlak, T. Engin, I. Calli, *Optimal design of MR damper via finite element analyses of fluid dynamic and magnetic field*, Mechatronics, vol. 22, no. 6, pp.890-903, Sep. 2012

[16] C. CHen, W.H. Liao, *A self-sensing magnetorheological damper with power generation*, Smart Mater. Struct., 21, p.025014, 2012

[17] G. Genta, L. Morello, *The Automotive Chassis, Vol.2 System Design*, Springer, 2009

[18] Reza N. Jazar, *Vehicle Dynamics: Theory and Application*, Springer, 2008

[19] L. Morello, L. Rosti Rossini, G. Pia, A. Tonoli, *The Automotive Body, Vol.II: System Design*, Springer, 2011

[20] Y. Zhang, K. Huang, F. Yu, Y. Gu, D. Li, *Experimental verification of energy-regenerative feasibility for an automotive elctrical suspension system*

[21] G. Zhang, J. Cao, F. Yu, *Design of active and regenerative controllers for DC motor-based suspension*, School of Mechanical Engineering, Shangai, Mechatronics 22, 1124-1134, 2012

[22] X.D.Xie, Q. Wang, *Energy harvesting from a vehicle suspension system*, Energy, Vol.86, 385-392, 2015

[23] Y. Kawamoto, Y. Suda, H. Ionue, T. Kondo, *Electro-mechanical suspension system considering energy consumption and vehicle maneuver*, Vehicle system design, Vol. 46, 1053-1063, Supplement, 2008

[24] Suda Y, Shiiba T, *A New Hybrid Suspension System with Active Control and Energy Regeneration*, Vehicle System Dynamics, 42(6), pp. 874-877, 1996

[25] D.A. Weeks, J.H. Beno, A.M. Guenin et al., *Electromechanical Active Suspension Demonstration for Off-Road Vehicles*, SAE, 2000

[26] J.H. Beno, D.A. Weeks, D.A. Bresie et al., *Experimental Comparison of Losses for Conventional Passive and Energy Efficient Active Suspension Systems*, SAE, 2002

[27] Zhongjie Li, Lei Zuo, J. Kuang, G. Luhrs, *Energy-Harvesting Shock Absorber with a Mechanical Motion Rectifier*, Smart Materials and Structures, 2012

[28] B. Huang, C.Y. Hsieh, F. Golnaraghi, M. Moallem, *A Methodology for Optimal Design of a Vehicle Suspension System with Energy Regeneration Capabilities*, Journal of Vibration and Acoustics, Vol. 137, 051014-1, October 2015

[29] Ling Zheng, Boyao Niu, Kan Wang, *The Integrated Design of Self-powered Magneto-Rheological Damper with Permanent Magnet Linear Generator*, ICSV21, Beijing, China, July 2014

[30] Chung-Neng Huang, Kuo-Han Chen, David T.W. Lin, *Development of a Novel Adaptive Suspension System based on Ball-screw Mechanism*, Applied Mechanics and Materials, Vols. 477-478, pp. 128-131, 2014

[31] Zhongjie Li, Lei Zuo, George Luhrs, Liangjun Lin, Yi-xian Qin, *Electromagnetic Energy-Harvesting Shock Absorbers: Design, Modeling, and Road Tests*, IEEE Transactions on vehicular technology, Vol.62, No.3, March 2013

[32] Y. Chen, Z.L. Wang, J. Qiu, H.Z. Huang, *Hybrid Fuzzy Skyhook Surface Control using Multi-Objective Microgenetic Algorithm for Semi-active Vehicle Suspension System Ride Comfort Stability Analysis*, J.Dyn. Sys., Meas., Control 134(4), 041003 (14pp), May 2012

[33] Peng Li, Chongxiao Zhang, Junyoung Kim, Liangyao Yu, Lei Zuo, *Buck-boost converter for simultaneous semi-active vibration control and energy harvesting for electromagnetic regenerative shock absorber*, Active and Passive Smart Structures and Integrted Systems, Vol. 9057, 2014

[34] *ISO Standards 2631*, 1997, Mechanical vibration and shock - Evaluation of human exposure to whole-body vibration

[35] U.S. Department of Transportation, *Average Annual Miles per Driver by Age Group*, http://www.fhwa.dot.gov/ohim/onh00/bar8.htm, as June 2016

[36] D. Karnopp, M.J. Crosby, R.A. Harwood, *Vibration control using semi-active force generators*, Journal of Engineering for Industry, 96(2):619-626, 1974

[37] M. Valek, M. Novk, Z. Ika, O. Vaculn, *Extended ground-hook new concept of semi-active control of truck's suspension*, Vehicle System Dynamics, 27(5-6):289-303, 1997

[38] National Highway Traffic Safety Administration, *An Assessment of Human Driver Steering Capability*, US Department of transportation, June 2005

[39] William L. Oberkampf, Timothy G. Trucano, *Verification and validation in computational fluid dynamics*, Progress in Aerospace Sciences, 38, pp. 209-272, 2002

[40] European Commission, Directorate-General Climate Action, The joint research center, *Technical Guidelines for the preparation of applications for the approval of innovative technologies pursuant to Regulation (EC) No 443/2009 of the European Parliament and of the Council*, February 2013

[41] FCA internal documentation

Appendix A: Correlation of CarSim and Simulink model

In this appendix, all the results coming from the simulations for the validation of the CarSim and Simulink model, which are not shown inside the thesis for sake of brevity, are presented. The results coming from the sine sweep test are shown in Figure 1. In this case, the parameters considering for the validation are: vertical acceleration measured at CG, longitudinal acceleration and pitch angle. The other quantities are not considered because of the fact that this test is done on a straight line and so the quantities are all null.

Concerning the double lane changes, all the quantities are evaluated, i.e. the vertical,

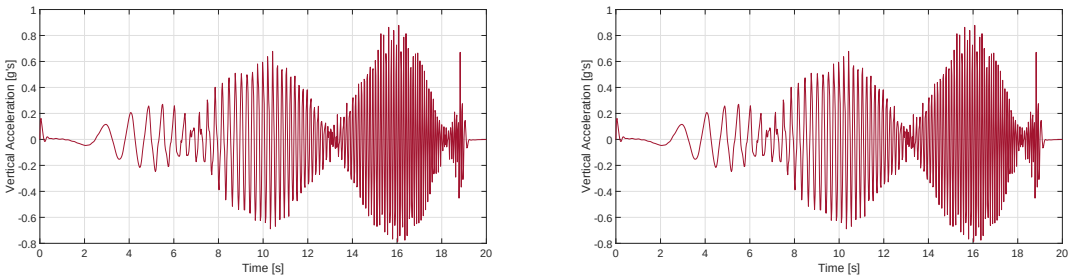

(a) *Vertical acceleration - Original model* **(b)** *Vertical acceleration - Modified model*

longitudinal and lateral accelerations and the pitch, roll and yaw angle. The results from the double lane change test are shown in Figure 2.

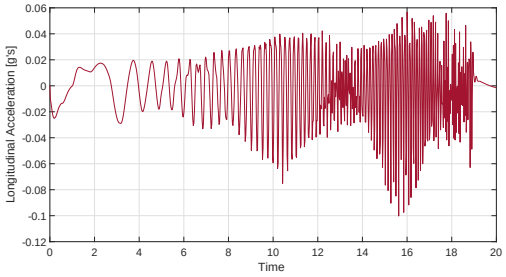

(c) *Longitudinal acceleration - Original model*

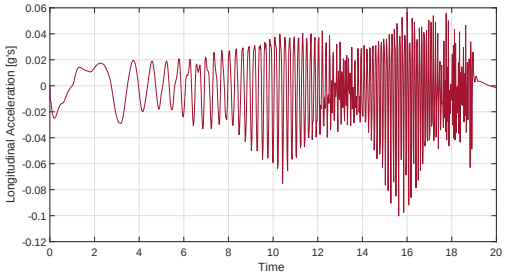

(d) *Longitudinal acceleration - Modified model*

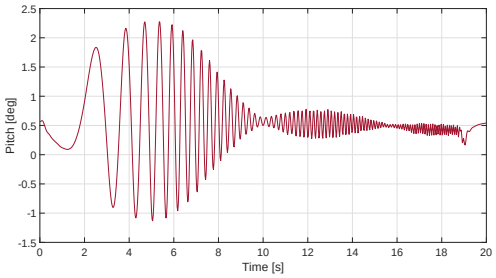

(e) *Pitch angle - Original model*

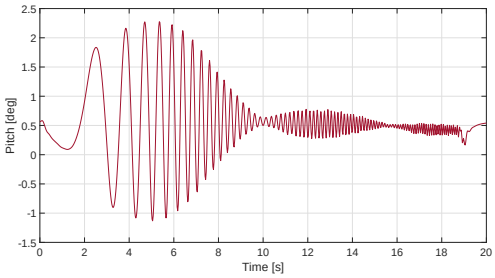

(f) *Pitch angle - Modified model*

Figure 1: *Model outputs - Sine sweep test*

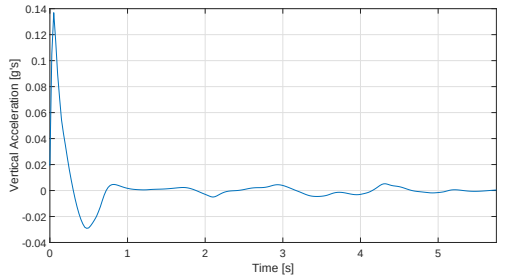

(a) *Vertical acceleration - Original model*

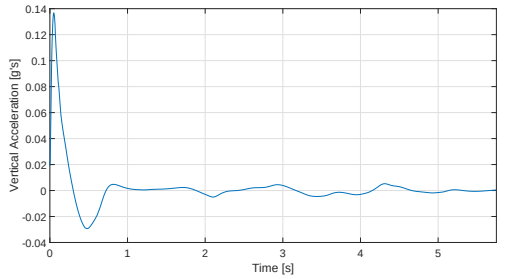

(b) *Vertical acceleration - Modified model*

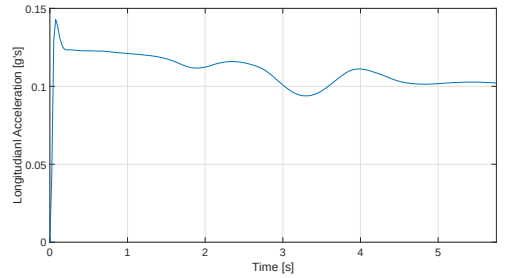

(c) *Longitudinal acceleration - Original model*

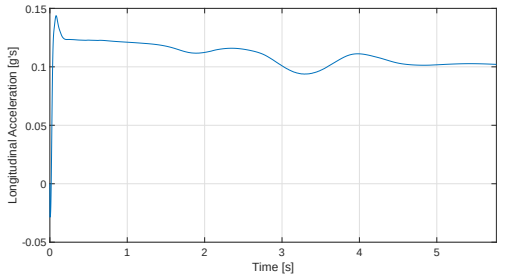

(d) *Longitudinal acceleration - Modified model*

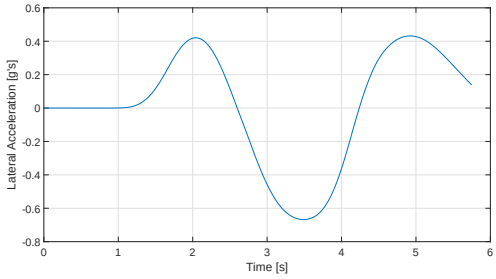

(e) *Lateral acceleration - Original model*

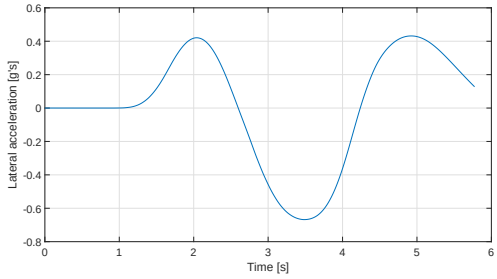

(f) *Lateral acceleration - Modified model*

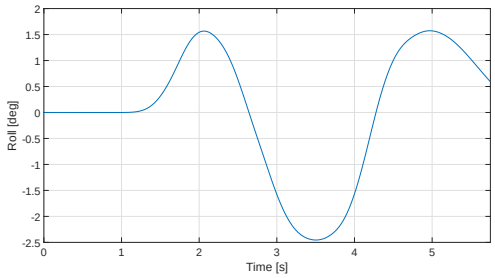

(g) *Roll angle - Original model*

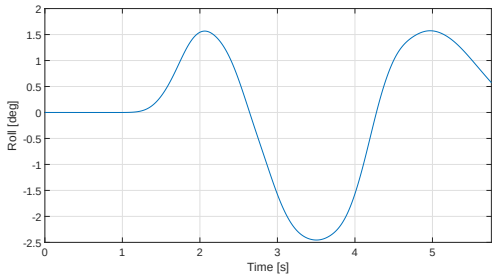

(h) *Roll angle - Modified model*

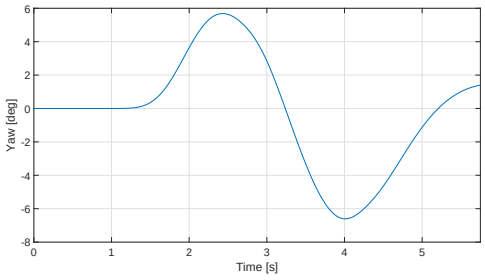

(i) *Yaw angle - Original model*

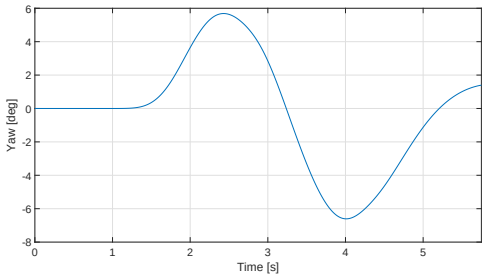

(j) *Yaw angle - Modified model*

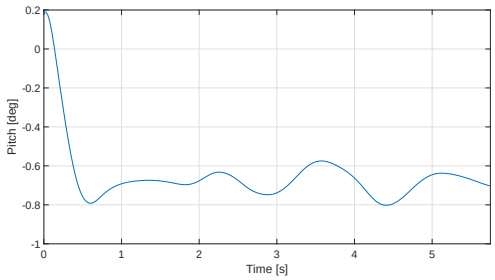

(k) *Pitch angle - Original model*

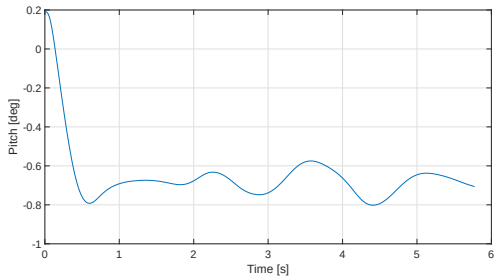

(l) *Pitch angle - Modified model*

Figure 2: *Model outputs - Double lane change*

Vita Auctoris

NAME:	Marco Di Vittorio
PLACE OF BIRTH:	Sant'Omero (TE), Italy
DATE OF BIRTH:	1992
EDUCATION:	Politecnico di Torino, B.Sc. in Automotive Engineering, Torino, Italy, 2014
	Politecnico di Torino, Master in Automotive Engineering, Torino, Italy, 2016
	University of Windsor, International M.A.Sc. in Mechanical Engineering, Windsor, Canada, 2016